Arylfluorenyl Substituted Metoxytriphenylamine Molecular Glasses for White and Blue Delayed-Fluorescence OLEDs Exploiting Green or Deep Blue Exciplexes

Monika Cekaviciute[1], Jurate Simokaitiene[1], Dmytro Volyniuk[1], Juozas V. Grazulevicius[1], Gjergji Sini[2]

[1]Department of Polymer Chemistry and Technology, Kaunas University of Technology, Radvilenu pl. 19, LT-50254, Kaunas, Lithuania; e-mail: juozas.grazulevicius@ktu.lt

[2] Laboratoire de Physicochimie des Polymeres et des Interfaces, EA 2528 Universite de Cergy-Pontoise, 5 mail Gay-Lussac, 95031 Cergy-Pontoise Cedex, France; e-mail: gjergji.sini@u-cergy.fr

Abstract: Arylfluorenyl-substituted triphenylamines were prepared by acid promoted Friedel-Crafts-type substitution reaction. The synthesized compounds were found to be capable of glass formation with glass transition temperatures above 152 ºC. The ionization potentials of the layers of the derivatives were found to be in the range of 5.25-5.41 eV. Time-of-flight hole drift and electron drift mobility values of the layer of tris[3-methoxy-4-(9-phenyl-9-fluorenyl)phenyl]amine (**2**) well exceeded 10^{-3} cm^2/Vs at high electric fields at room temperature. The synthesized compounds showed exciplex-forming properties. The deep blue exciplex based thermally activated delayed fluorescence emitters with the CIE chromaticity coordinates of (0.179; 0.104) are described. The exciplex emitters were utilized in the cold-white and deep-blue organic light-emitting diodes of the simple structures using only exciplex emitters. The devices showed external quantum efficiency of 2.55% and 1.2 %, respectively. Results obtained by means of density functional theory (DFT) calculations were used to discuss on the charge-transporting and optical properties of the compounds.

Keywords: fluorene, triphenylamine, molecular glasses, bipolar charge-transport, WOLED

1. Introduction

White organic light-emitting diodes (WOLEDs) are good candidates for solid-state illumination and display technologies[1,2]. Compered to inorganic white light-emitting diodes (LEDs), WOLEDs can be fabricated as transparent, large-area, flexible, lightweight devices[3]. They are characterized by low turn-on voltage, a wide viewing angle, fast response, high brightness. However, the efficiency and life-time of organic light-emitting diodes (OLEDs) are still lower than those of white LEDs[4]. In order to achieve maximum external quantum efficiency (η_{ext}) in OLEDs, several important parameters entering equation 1 are required to be equal to unity[5,6]:

$$\eta_{ext}=\gamma\times\phi_{PL}\times\chi\times\eta_{out} \qquad \text{(Eq. 1)}$$

In this equation, γ corresponds to the charge-balance factor, ϕ_{PL} is the photoluminescence quantum efficiency, χ is the efficiency of exciton production, and η_{out} corresponds to the outcoupling efficiency. High γ values could be provided in well-constructed OLEDs using additional layers such as hole- and electron-transporting layers with high charge mobilities and appropriate energy levels[7,8]. The photophysical properties of the emitter molecules define the value of ϕ_{PL} which must be close to 1. The outcoupling efficiency η_{out} can be significantly increased using multifunctional anode stacks, a high-refractive-index substrates, or a periodic outcoupling structure[9,10]. The exciton production efficiency (χ) generated by electrical injection depends on the molecular structures of the organic emitters. In the case of fluorescent organic emitters harvesting only the singlet excitons χ=0.25, thus limiting the internal quantum efficiency (η_{in}) of fluorescent OLEDs on the level of 25 %. Both the singlet (25%) and triplet (75%) excitons can be harvested in phosphorescent organic emitters which contain rare-earth metal atoms such as iridium, platinum, or osmium. Very effective phosphorescent WOLEDs were reported, however, many of them contain blue fluorescent emitters, since most of the known blue phosphorescent emitters are not sufficiently stable[10,11]. In addition, exploitation of rare-earth-metal-based compounds as phosphorescent emitters is problematic because of the environmental reasons and of high cost.

A new generation of organic emitters for OLEDs based on thermally activated delayed fluorescence (TADF) was recently discovered[12]. TADF can be generated in emitters exhibiting charge-transfer (CT) between donor (D) and acceptor (A) moieties, provided that extremely small singlet-triplet energy gap (ΔE_{ST}) can be obtained. Such emitters allow harvesting of triplet excitons through efficient intersystem crossing (ISC) between triplet and singlet levels, resulting in χ values approaching unity. Both intramolecular and intermolecular CT can lead to TADF in organic materials[12]. The intramolecular CT was observed in emitters containing pretwisted D and

A moieties combined in one molecule which usually is not easy to synthetize[12]. The intermolecular CT was observed between exciplex forming D and A molecules which are simply mixed together[13]. The exciplex emission is shifted to lower-energy spectral region compared to the emission of D or A molecules. Therefore, most of the reported exciplex-based devices emit green or red light[13-15]. Orange- or yellow exciplex emitters are successfully employed in WOLEDs[16,17].

Blue TADF molecules as well as blue TADF exciplex molecular mixtures with emission maxima close to 470 nm were also reported[18,19]. Bis[4-(9,9- dimethyl-9,10-dihydroacridine)phenyl]sulfone with emission maximum at 470 nm was, for instance, used in highly efficient WOLED as a blue TADF emitter in combination with green and red fluorescent emitters[20]. Blue TADF exciplex between a donor 1,3- bis(N-carbazolyl)benzene and a acceptor ((1,3,5-triazine-2,4,6-triyl)tris(benzene-3,1-diyl))tris(diphenylphosphine oxide) (PO-T2T) was also reported[21]. Hybrid WOLED was fabricated using this blue exciplex and an orange phosphorescence dopant bis(2-phenyl-1,3-benzothiozolato-N,C2') iridium (acetylacetonate)[22] showing that to produce white light in WOLEDs not only TADF but also phosphorescence emitters were used. An example of full TADF-based WOLED including blue and orange exciplexes was recently published[21]. However, that WOLED had extremely complicated structure with the active layer composed of more than ten layers including two individual host-guest layers and an inorganic layer[21]. Therefore, the search for both new approaches of simplifying of OLED structures and new TADF emitters for efficient blue OLEDs and WOLEDs is still an urgent problem.

Derivatives of triphenylamine (TPA) represent one of the largest classes of organic electroactive materials[23]. They have been successfully used as components of optoelectronic devices and OLEDs in particular[24-27]. Chemical modifications such as introduction of methoxy groups into the structures of organic semiconductors or attachment of electron-donating moieties to triphenylamine group can lead respectively to the decrease of their ionization potentials[28] and to the formation of bipolar materials capable of effectively transporting both holes and electrons[29,30].

Fluorene-triphenylamine hybrids are synthesized via simple one-step procedure from commercially available starting compounds[31,32].These compounds have high glass transition temperatures, high thermal and electrochemical stabilities[33]. The fluorene-triphenylamine hybrid (tris[4-(9-phenylfluoren-9-yl)phenyl]amine has been used as a host material in full-color elctrophosphorescent devices[31].

In this work we report on the synthesis and properties of star-shaped phenylfluorenyl-substituted methoxytriphenylamine derivatives. A new approach for the fabrication of WOLEDs based on a deep blue exciplex and a green exciplex is also investigated. Our WOLEDs are composed of only three active layers containing three materials (emitting, hole and electron transporting ones). Deep blue exciplexes with the deepest emission maxima situated at 427 nm were identified in the mixtures of our new arylfluorenyl-substituted metoxytriphenylamine derivatives and 4,7-diphenyl-1,10-phenanthroline (Bphen) or 2,9-dimethyl-4,7 diphenyl-1,10-phenanthroline (BCP). In our WOLEDs, green emission was obtained by means of the well-known TADF exciplexes between 4,4′,4″-tris[3-methylphenyl(phenyl)amino] triphenylamine (m-MTDATA) and Bphen or BCP[34,35]. The choice of m-MTDATA:Bphen exciplex emitter[36] was motivated by the high η_{ext} value (7.79%) and by the deep blue with CIE chromaticity coordinates of (0.179; 0.104) obtained in OLED based on this exciplex.

2. Experimental

2.1. Materials

All the required chemicals, i.e. 4-bromoanisole, 9-fluorenone, magnesium, 9-phenyl-9-fluorenol, trifluoromethanesulfonic acid (CF_3SO_3H), 4,4′,4″-tris[3-methylphenyl(phenyl)amino]triphenylamine (m-MTDATA), bathophenanthroline (BPhen) and 2,9-dimethyl-4,7-diphenyl-1,10-phenanthroline (BCP) were obtained from Sigma-Aldrich and used as received. 2,2’,2’’-Trimethoxytriphenylamine (Mp = 144-147 ºC, lit. Mp = 139.5-140 ºC[37]) and 3,3’,3’’-trimethoxytriphenylamine were obtained under Ullmann conditions[38,39]. 9-(4-Methoxyphenyl)-9-fluorenol was synthesized according to previously described procedure[40].

Tris[2-methoxy-4-(9-phenyl-9-fluorenyl)phenyl]amine (1) 2,2’,2’’-Trimethoxytriphenylamine (0.42 g, 1.25 mmol) and 9-phenyl-9-fluorenol (1 g, 3.87 mmol) were dissolved in 1,4-dioxane (40 ml). Trifluoromethanesulfonic acid (CF_3SO_3H, 0.48 g, 3.19 mmol) was added drop wise to the stirred reaction mixture under argon atmosphere. The reaction mixture was heated up to 80 ºC and kept at this temperature for 4 h. When the reaction was finished (TLC control) the reaction mixture was cooled, neutralized with aqueous sodium hydroxide solution and extracted with dichloromethane. The organic extracts were washed with water and dried (Na_2SO_4) the solvent was evaporated under vacuum. The product was purified by silica gel column chromatography using an eluent mixture of tetrahydrofuran and hexane in the volume ratio of 5:1. It was recrystallized from the mixture of methanol and dichloromethane. The yield of white crystals was 23 % (0.3g). Mp = 305-308 ºC.

MS (APCI+, 20V), m/z(%): 1056 ($[M+H]^+$, 55).

^{1}H NMR (300 MHz, DMSO-d_6) δ (ppm): 3.22 (s, 9H), 6.54 (s, 6H), 6.62 (s, 3H), 7.03-7.06 (m, 6H), 7.17-7.30 (m, 15H), 7.34-7.43 (m, 12H), 7.89 (d, *J* = 7.5 Hz, 6H).

^{13}C NMR (75.4 MHz, DMSO-d_6) δ (ppm): 56.46, 65.35, 108.18, 114.46, 121.17, 125.05, 126.77, 127.31, 128.19, 128.34, 128.48, 128.99, 136.49, 140.21, 141.35, 146.53, 151.31, 153.23.

IR ν_{max} (KBr): 3058, 3017 (C-H, Ar), 2961, 2930 (C-H), 2831 (OCH_3), 1505, 1448 (C=C, Ar), 1281 (C-O-C).

Tris[3-methoxy-4-(9-phenyl-9-fluorenyl)phenyl]amine (2) was prepared by the similar procedure as compound **1** using 3,3',3''-trimethoxytriphenylamine (0.32 g, 0.95 mmol), 9-phenyl-9-fluorenol (0.76 g, 2.94 mmol) and CF_3SO_3H (0.39 g, 2.59 mmol). The product was purified by silica gel column chromatography using an eluent mixture of tetrahydrofuran and hexane in the volume ratio of 5:1. It was recrystallized from mixture of methanol and dichloromethane. The yield of white crystals was 43 % (0.44g). Mp = 282-286 ºC.

MS (APCI+, 20V), m/z(%): 1056 ($[M+H]^+$, 10).

^{1}H NMR (300 MHz, DMSO-d_6) δ, (ppm): 3.21 (s, 9H), 6.37 (dd, J_1 = 2.2 Hz, J_2 = 8.5 Hz, 3H), 6.62 (d, *J* = 8.5 Hz, 3H), 6.67 (d, *J* = 2.2 Hz, 3H), 6.95-6.98 (m, 6H), 7.07-7.14 (m, 9H), 7.21(t, *J* = 7.5 Hz, 6H), 7.33(t, *J* = 7.4 Hz, 6H), 7.50 (d, *J* = 7.5 Hz, 6H), 7.85 (d, *J* = 7.5 Hz, 6H).

^{13}C NMR (75.4 MHz, DMSO-d_6) δ (ppm): 55.98, 63.91, 109.78, 115.99, 120.95, 126.00, 126.41, 126.94, 128.21, 128.38, 128.49, 128.69, 129.71, 140.21, 146.56, 147.59, 151.46, 159.37.

IR ν_{max} (KBr): 3054, 3017 (C-H, Ar), 2928 (C-H), 2830 (OCH_3), 1595, 1492, 1447 (C=C, Ar), 1217 (C-O-C).

Tris{2-methoxy-4-[9-(4-methoxyphenyl)-9-fluorenyl]phenyl}amine (3) was prepared by the similar procedure as compound **1** using 2,2',2''-trimethoxytriphenylamine (0.65 g, 1.94 mmol), 9-(4-methoxyphenyl)-9-fluorenol (2.67 g, 9.26 mmol) and CF_3SO_3H (1.21 g, 8.06 mmol).The product was purified by silica gel column chromatography using an eluent mixture of ethyl acetate and hexane in the volume ratio of 1:6. White powder was obtained after precipitation in methanol with the yield of 22 % (0.49g).

MS (APCI+, 20V), m/z(%): 1146 ($[M+H]^+$, 45).

^{1}H NMR (400 MHz, $CDCl_3$) δ (ppm): 3.25 (s, 9H,), 3.72 (s, 9H), 6.55 (dd, J_1 = 1.9 Hz, J_2 = 8.3 Hz, 3H), 6.60 (d, *J* = 8.3 Hz, 3H), 6.64 (d, *J* = 1.8 Hz, 3H), 6.71 (d, *J* = 8.9 Hz, 6H), 7.07 (d, *J* = 8.9 Hz, 6H), 7.22 (t, *J* = 7.5 Hz, 6H), 7.31 (t, *J* = 7.5 Hz, 6H), 7.36 (d, *J* = 7.6 Hz, 6H), 7.72 (d, *J* = 7.5 Hz, 6H).

^{13}C NMR (100 MHz, $CDCl_3$) δ (ppm): 55.01, 55.53, 64.44, 113.23, 119.88, 120.43, 123.96, 125.92, 127.07, 127.31, 128.93, 128.95, 135.89, 138.04, 139.82, 140.82, 151.61, 157.97, 158.04.

IR ν_{max} (KBr): 3058, 3034 (C-H, Ar), 2930 (C-H), 2832 (OCH_3), 1506, 1447 (C=C, Ar), 1248 (C-O-C).

Tris{3-methoxy-4-[9-(4-methoxyphenyl)-9-fluorenyl]phenyl}amine (4) was prepared by the similar procedure as compound **1** using 3,3',3''-trimethoxytriphenylamine (0.3 g, 0.89 mmol), 9-(4-methoxyphenyl)-9-fluorenol (0.87 g, 3.02 mmol) and CF_3SO_3H (0.36 g, 2.40 mmol). The product was purified by silica gel column chromatography using an eluent mixture of tetrahydrofurane and hexane in the volume ratio of 1:6. White powder was obtained after precipitation in methanol with the yield of 25 % (0.26g).

MS (APCI+, 20V), m/z(%): 1147 ($[M+H]^+$, 100).

^{1}H NMR (400 MHz, $CDCl_3$) δ (ppm): 3.31 (s, 9H), 3.72 (s, 9H), 6.38 (dd, J_1 = 8.5 Hz, J_2 = 2.1 Hz, 3H), 6.62 (d, J = 2.1 Hz, 3H), 6.68-6.73 (m, 9H), 7.01 (d, J = 8.8 Hz, 6H), 7.22 (t, J = 7.6 Hz, 6H), 7.32 (t, J = 7.3 Hz, 6H), 7.55 (d, J = 7.5 Hz, 6H), 7.72 (d, J = 7.5 Hz, 6H).

^{13}C NMR (100 MHz, $CDCl_3$) δ (ppm): 55.17, 55.49, 63.08, 109.09, 113.23, 115.747, 119.88, 126.46, 127.01, 127.18, 127.464, 128.17, 129.64, 138.16, 140.03, 147.37, 151.87, 157.62, 158.97.

IR ν_{max} (KBr): 3056, 3032 (C-H, Ar), 2930 (C-H), 2832 (OCH_3), 1596, 1508, 1447 (C=C, Ar), 1246 (C-O-C).

2.2. Methods

^{1}H NMR and ^{13}C NMR spectra were recorded with Varian Unity Inova [300 MHz (^{1}H), 75.4 MHz (^{13}C)] and Bruker Avance III [400 MHz (^{1}H), 100 MHz (^{13}C)] spectrometers at room temperature. All the data are given as chemical shifts δ (ppm) downfield from $Si(CH_3)_4$. Infrared (IR) spectra were recorded using PerkinElmer Spectrum GX II FT-IR System. The samples of the solid compounds were prepared in the form of KBr pellets. Mass spectrometry (MS) was performed with the Bruker maxis 4G. Differential scanning calorimetry (DSC) measurements were carried out in a nitrogen atmosphere with a Perkin Elmer at DSC 8500 equipment at a heating and cooling rate of 10 °C/min. Thermogravimetric analysis (TGA) was performed on a Perkin Elmer TGA 4000 apparatus in a nitrogen atmosphere at a heating rate of 20 ºC/min. Melting points were measured with Electrothermal MEL-TEMP melting point apparatus. Absorption spectra of dilute (10^{-5} M) solutions in tetrahydrofuran (THF) were recorded on an UV−vis−NIR spectrometer Lambda 950 (Perkin-Elmer). Fluorescence spectra, fluorescence quantum yields (Φ_{FL}) and fluorescence decay curves of dilute solutions in THF or toluene (10^{-5} M) and of solid films of the compounds were recorded with Edinburgh Instruments LS980 spectrometer. Using an AvaSpec-2048 XL spectrometer, phosphorescence spectra were recorded

with >100 μs delay after excitation. Cyclic voltammetry (CV) measurements were carried out using a micro-Autolab III (Metrohm Autolab) potentiostat-galvanostat equipped with a standard three-electrode configuration. A three-electrode cell equipped with a glassy carbon working electrode, an Ag/Ag (0.01 M in anhydrous acetonitrile) reference electrode and a Pt wire counter electrode were employed. The measurements were done in anhydrous dichloromethane with tetrabutylammonium hexafluorophosphate (0.1 M) as the supporting electrolyte under nitrogen atmosphere at a scan rate of 0.1 V/s[41-43]. The measurements were calibrated using an internal standard, ferrocene/ferrocenium (Fc) system. The oxidation potentials ($E_{1/2}$ vs Fc) for the reversible oxidation were taken as the average values of the anodic and cathodic peak potentials, Epa and Epc, respectively. Ionization potentials (I_P^{ep}) of the films of the synthesized compounds were measured by electron photoemission in air method as described before[44]. Hole drift mobilities were studied by a time of-flight (ToF) method[45,46]. For both the electron photoemission and ToF measurements, the vacuum-deposited layers of the studied compounds were prepared.

OLEDs based on doped emitting layer with the following architectures were fabricated: ITO/m-MTDATA(30 nm)/70 wt% **2**:30 wt% BPhen(25 nm)/BPhen(25 nm)/Ca(10 nm)/Al(60 nm) (designated as WhiteD1), and ITO/m-MTDATA(30 nm)/**2**(8 nm)/30 wt% **2**:70 wt% BPhen(25 nm)/BPhen(25 nm)/Ca(10 nm)/Al(60 nm) (designated as BlueD). Before deposition of the layers, the ITO-coated glass substrates with a sheet resistance of 15 Ω/sq were cleaned in acetone and isopropyl alcohol ultrasonic baths during ca. 10 min. The organic layers, calcium and aluminum films were vacuum-deposited under the vacuum of $2\text{-}5\times10^{-6}$ mBar using vacuum equipment from Kurt J. Lesker in-built in an MB EcoVap4G glove box.

2.3. Computational Details

All computations were performed at the density functional theory (DFT) level[47] employing the B3LYP[48,49] functional, in conjunction with the 6-31G(d,p) basis set. The spectroscopic properties of the molecules were calculated using a time dependent density functional theory method (TDDFT)[50-53] in the absence of medium effects. Up to 20 excited states were calculated and the theoretical absorption bands were obtained by considering a band half-width of 0.2 eV at half-height[54]. The vertical and adiabatic ionization potentials (*Ip*) were calculated ‘‘in the gas phase’’ at the B3LYP/6-31G (d,p) level as the differences of the total energies between the neutral species and the cationic species. The internal reorganization energy (λ_i) values were calculated at the B3LYP/6-31G(d,p) level according to the following equation[55]:

$$\lambda_i = \lambda_i^1 + \lambda_i^2 = \left(E_M^{Geom(M^+)} - E_M^{Geom(M)}\right) + \left(E_{M^+}^{Geom(M)} - E_{M^+}^{Geom(M^+)}\right)$$

in which the quantity $E_{M^+}^{Geom(M)}$ for instance corresponds to the energy of the cationic species (M^+) in the geometry of the neutral molecule (M). All computations were performed with the Gaussian 09 program[56].

3. Results and Discussion

3.1. Synthesis

The synthetic route towards the appropriate arylfluorenyl substituted triphenylamines is shown in Scheme 1. Compounds **1–4** were obtained by Friedel-Crafts-type substitution reaction[31]. All the compounds were purified by column chromatography. They were identified by IR-, ^{1}H NMR-, ^{13}C NMR- and mass spectrometries.

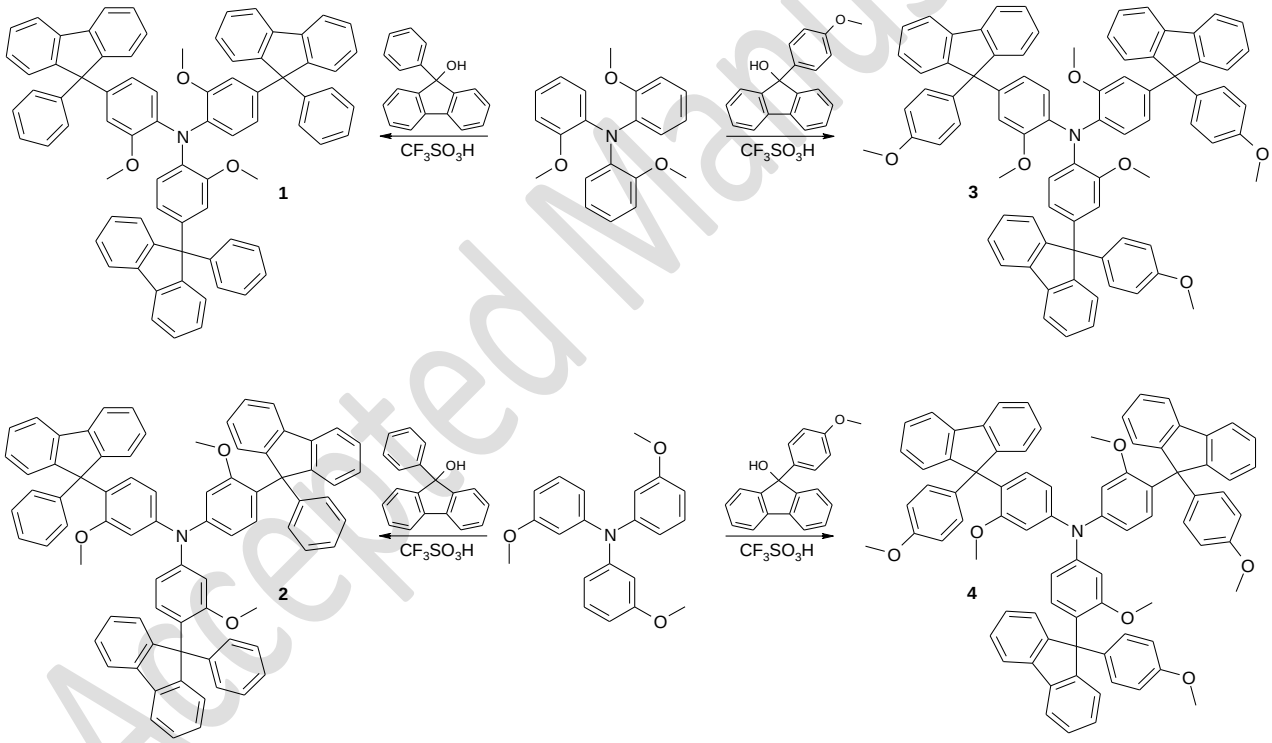

Scheme 1. Syntheses scheme of compounds **1**–**4**.

3.2. Geometries of Compounds and Frontier Orbitals

The geometries of compounds **1–4** were determined theoretically. The geometries of the two *o*-methoxytriphenylamine-based compounds (**1**, **3**) are similar between them. A similar observation applies to *m*-methoxytriphenylamine-based compounds (**2**, **4**), so that only the geometries of compounds **1** and **2** are shown in Figure 1. The propeller-like TPA core has pitch-of-blade angles (a) ranging 57º–59º and 39º–41º in *ortho*-methoxy substituted compounds (**1**, **3**) and in *meta*-

methoxy substituted compounds (**2**, **4**) respectively. Each TPA phenyl group has two substituents in the *para* position – fluorenyl and phenyl (methoxyphenyl). As expected, smaller phenyl-phenyl dihedral angles with average values of ~ 40° and ~ 44° were found for compounds **1**, **3** and **2**, **4** respectively, as compared to phenyl-fluorenyl ones (~ 90° and ~ 85° for **1**, **3** and **2**, **4** respectively, average values). The larger dihedrals found for the fluorenyl moieties are due to the larges steric repulsions, which are expected to impact the distribution of frontier orbitals and the electronic- and optical properties related to these orbitals.

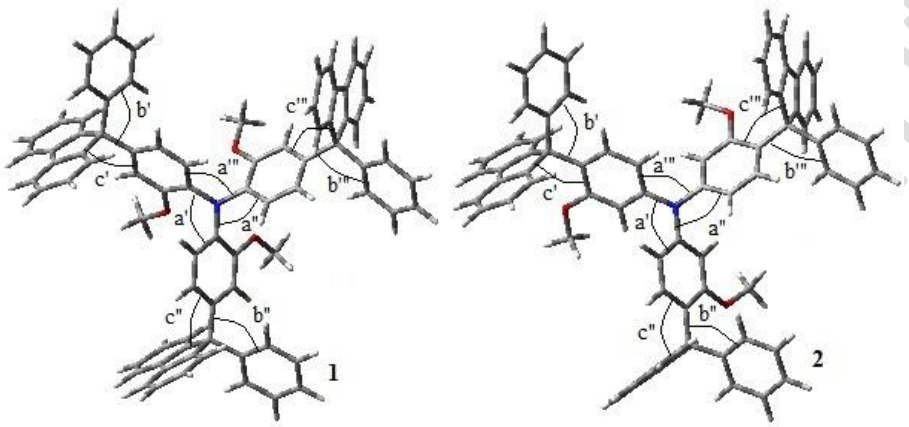

Figure 1. Geometries for compounds **1** and **2** obtained by gas phase calculations at the B3LYP/6-31G(d,p) level.

The frontier orbitals for the synthesized molecules were found to be very similar (Figure 2). HOMO is localized on the triphenylamine core and LUMO is localized on one of fluorene sidearms. The electronic properties related to these orbitals are consequently expected to exhibit similarities. The localization of the frontier orbitals in different moieties is due to a cumulated effect of the energy difference between the local HOMOs (LUMOs) of each fragment, and to the almost orthogonal space orientation, in turn stemming from their steric repulsion.

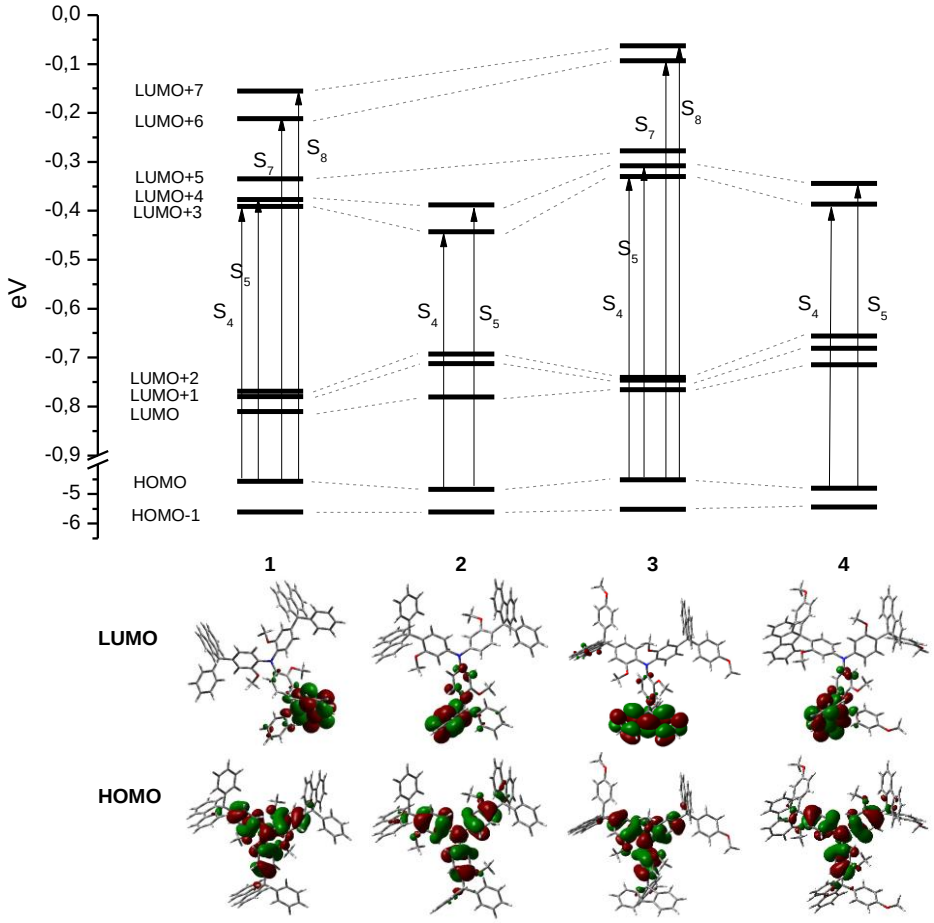

Figure 2. Energy diagram corresponding to HOMO-1 through LUMO+7 molecular orbitals of compounds **1**–**4** obtained at the B3LYP/6-31G(d,p) level. The dominant electronic transitions corresponding to select excited states are indicated with vertical arrows. Pictograms of HOMO and LUMO orbitals corresponding to compounds **1**–**4** are also shown.

3.3. Thermal Properties

The thermal characterization of the compounds was performed by DSC and TGA under a nitrogen atmosphere. The thermal characteristics are summarized in Table 1. All the synthesized compounds (**1**–**4**) showed high thermal stability. The temperatures of the onsets of the thermal degradation (T_{dec}) were above 415 ºC, as confirmed by TGA with a heating rate of 20 ºC/min. The thermal stability of *m*-methoxytriphenylamine-based compounds (**2**, **4**) was found to be higher than that of *o*-methoxytriphenylamine-based compounds (**1**, **3**) (Figure 3). Compounds **3** and **4** having additional methoxy groups in phenylfluorenyl moieties showed slightly lower thermal stabilities than their corresponding counterparts having without additional methoxy groups (**1** and **2**). Compounds **1** and **2** were isolated after the synthesis as crystalline substances however they could be transformed into the glassy state by heating from the melts or by casting from the solutions. Compounds **3** and **4** were obtained as white amorphous powders. They

showed only glass transitions both in the heating and in the cooling DSC scans. All the synthesized arylfluorenyl substituted methoxytriphenylamines (**1**–**4**) showed high glass transition temperatures (T_g) which ranged from 151 to 165 ºC. The comparison of the values of T_g of compounds **1** and **2** with those of compounds **3** and **4** allows to conclude that methoxy groups in the peripheral phenyl moieties does not result in any substantial reduction of T_g. Glass transition temperatures of *meta*-methoxy substituted compounds (**2**, **4**) were found to be higher by ca. 10 ºC than those of *ortho*-methoxy substituted compounds (**1**, **3**).

Table 1. Thermal characteristics of compounds **1**–**4**.

Compound	$T_{cr.}$, ºC	$T_{m.}$, ºC	T_g[a], ºC	T_{dec}[b], ºC
1	285	317	152	424
2	-	293	165	478
3	-	-	151	415
4	-	-	162	440

T_m , $T_{cr.}$, T_g estimated by DSC: scan rate, 10 ºC/min; N_2 atmosphere; [a] second heating scan. T_{dec} estimated by TGA at a heating rate of 20 ºC/min; N_2 atmosphere.

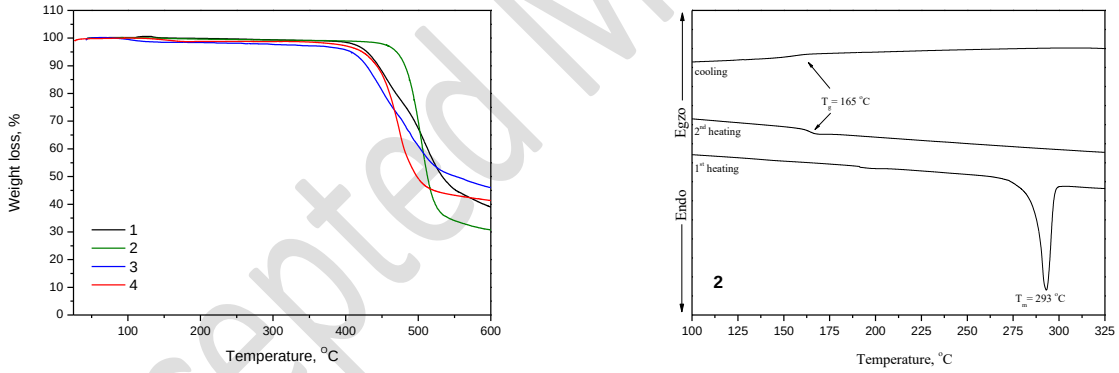

Figure 3. TGA curves of arylfluorenyl substituted triphenylamines **1**–**4** recorded at a heating rate of 20 ºC/min in nitrogen atmosphere. DSC curves of compound **2** at a recorded heating rate of 10 ºC/min in nitrogen atmosphere.

3.4. Electrochemical and Photoelectrical Properties

The electrochemical properties of the compounds were studied by cyclic voltammetry (CV). The cyclic voltammograms of **1**–**4** showed the reversible oxidation with the peak height varying linearly with sweep rate and the same values of anodic and cathodic peak currents (Figure 4). The shape of cyclic voltammograms was found to be similar for all the studied compounds. The electrochemical data are summarized in Table 2. The ionization potential values (I_p^{cv}) were

determined from the values of the first oxidation potential with respect to ferrocene (Fc). The ionization potential values (I_p^{cv}) of the synthesized compounds were found to be close and ranged from 5.11 to 5.26 eV. The electron affinities (EA^{cv}) determined from the optical energy band gaps (E_g^{opt}) and ionization energy values ranging 1.60–1.75 eV.

The ionization potentials (I_p^{ep}) of the solid layers of compounds **1**–**4** were also established, by electron photoemission spectrometry in air. The electron photoemission spectra are shown in Figure 5. The values of I_p^{ep} are given in Table 2. The I_p^{ep} values ranging 5.25–5.41 eV are slightly larger than the electrochemical values, however, the trend is similar in both set of values. The ionization potential values of *ortho*-methoxy-substituted triphenylamine derivatives (**1**, **3**) were found to be a little lower than those of *meta*-methoxy-substituted counterparts (**2**, **4**). Similar dependency of I_p^{ep} on the position of methoxy groups was earlier observed for 1,1-bis(4-aminophenyl)cyclohexane based arylamines[28]. A similar I_p trend can be deduced also from the HOMO energy values (Table 2). The smaller I_p values of the *ortho*-isomers as compared to *meta*-ones is due to the distribution of HOMO in the TPA phenyl groups, exhibiting large coefficients at the *ortho* positions, and almost zero coefficients at the *meta* position, thus responding differently to the antibonding interactions with the methoxy groups. This effect is almost absent in the case of peripheral methoxy groups due to the strict HOMO localization on the TPA moieties, which can explain the negligible impact of the methoxy groups on the I_p values of compounds **3** and **4** as compared to **1** and **2**.

Table 2. I_p, EA, E_g energies of compounds **1**–**4**.

Compound	$E_{1/2}$ vs Fc, V	E_g^{opt},[a] eV	I_p^{cv},[b] eV	EA^{cv},[c] eV	I_p^{ep},[d] eV	ε_{HOMO},[e] eV	ε_{LUMO},[e] eV
1	0.32	3.51	5.12	1.61	5.25 (5.50)	-4.57	-0.81
2	0.46	3.51	5.26	1.75	5.41 (5.79)	-4.84	-0.78
3	0.31	3.51	5.11	1.60	5.26 (5.43)	-4.52	-0.77
4	0.44	3.58	5.24	1.66	5.40 (5.73)	-4.80	-0.72

[a] The optical band gap estimated from the edges of electronic absorption spectra

[b] The ionization potentials measured by electrochemical studies $I_p^{cv}=4.8+E_{1/2}$vsFc[43].

[c] The electron affinities calculated using equation $EA^{cv}= I_p^{cv} - E_g^{opt}$.

[d] The ionization potentials measured by electron photoemission in air method; in parenthesis theoretical adiabatic I_p values obtained at B3LYP/6-31G(d,p) level "in gas phase".

[e] HOMO and LUMO energies calculated at the B3LYP/6-31G(d,p) level "in gas phase".

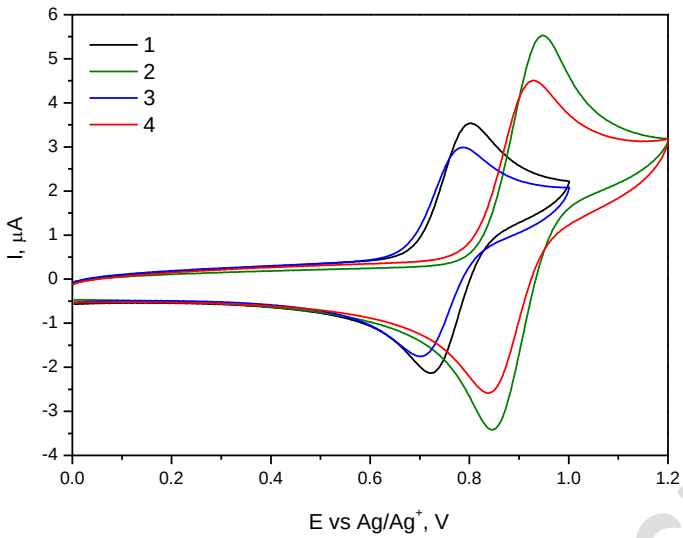

Figure 4. Cyclic voltammograms of dilute solutions of compounds **1**–**4** in dichloromethane at 25 °C at sweep rate of 0.1 V/s.

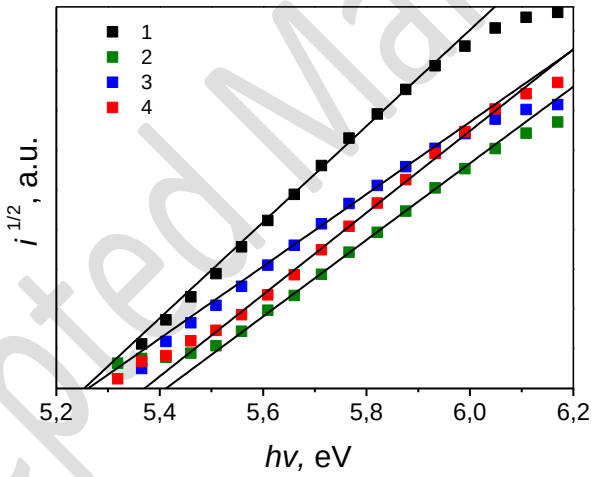

Figure 5. Electron photoemission spectra of the films of compounds **1**–**4** recorded in air at 25 °C.

3.5. Optical and Photophysical Properties

Absorption and fluorescence spectra of compounds **1**–**4** are shown in Figure 6. The spectral data are collected in Table 3. The absorption spectra of the dilute solutions in THF of arylfluorenyl-substituted derivatives **1**–**4** are similar and display two absorption bands at ca. 270 and 310 nm originated mainly from the absorptions of the fluorene moieties and the triphenylamine core, respectively. The theoretical absorption spectra (Figure 7) of **1**–**4** indicate that the maxima of absorption bands result as a combination of electronic transitions towards several excited states.

The HOMO→LUMO, LUMO+1 transitions ($S_0 \rightarrow S_1$, S_2) are of charge transfer character (Figure 2). In Figure 7, these transitions are of small oscillator strength and energetically close to the strong of intra-triphenylamine transitions. $S0 \rightarrow S_1$, S_2 transitions are consequently hidden and do not appear as a separate band. The intense low energy band of *ortho*-methoxy substituted compounds (**1** and **3**) is due to HOMO→LUMO+3, LUMO+4, LUMO+6 and LUMO+7 transitions, which are of mixed charge transfer and local excitation nature (see Figure S1, SI, for the pictograms of the corresponding orbitals). A similar observation applies to the nature of the low energy band for *meta*-methoxy-substituted compounds (**2** and **4**). As expected, the impact of the peripheral methoxy groups in the absorption spectra is negligible, which is due to the negligible contribution of the methoxy-phenyl groups in the HOMO and the virtual orbitals involved in the corresponding transitions (Figure S1).

Similarly to the absorption spectra, the introduction of methoxy groups into phenylfluorenyl substituents does not substantially affect the fluorescence spectra of the dilute solutions. (cf. the spectra of the solutions of **3** and **4** with those of **1** and **2**). Fluorescence intensity maxima of dilute solutions in THF of the compounds with *o*-methoxytriphenylamine core (**1**, **3**) exhibit bathochromic shifts compared to those of the compounds with *m*-methoxytriphenylamine core (**2**, **4**). The Stokes shifts range 60–97 nm (48–78 meV) in THF, indicating increase in the dipole moments (DM) between the ground state (GS) and the first excited state S_1 ($\Delta\mu$). Our calculations indeed result in $\Delta\mu$ values in gas phase ranging 20-24 Debye (Table S1). The larger Stokes shifts by roughly 34–36 nm (27–29 meV) in the case of compounds **1**, **3** as compared to **2**, **4** can be due to a combination of two effects: (i) larger difference in the dipole moments (DM) between the ground state (GS) and S_1 for *ortho*-methoxy substituted compounds (**1**, **3**) than for *meta*-methoxy substituted compounds (**2**, **4**). (ii) The intramolecular relaxation energy in the S_1 state might be more important for *ortho*-methoxy-substituted compounds (**1**, **3**) than for *meta*-methoxy-substituted compounds (**2**, **4**). Both factors seem to contribute equally, as the Stokes shifts for ortho compounds in toluene (small dielectric constant) are roughly 19 nm (15 meV) larger than for the meta compounds, which is almost half of the difference in Stokes shift in THF.

The emission intensity maxima of the solutions in THF showed red shifts with respect to those of the solutions in toluene (Figure 6). This solvatochromic effect is larger (25 nm) in the case of *ortho*-methoxy-substituted compounds **1** and **3**, and much smaller (6 nm) for the *meta*-methoxy-substituted compounds **2** and **4**. Again, this observation can be explained by the larger increase in the S_1 dipole moment as compared to the GS one for the former compounds, in correlation with different polarity of the media. The emission spectra of the solid films of compounds **1**–**4**

were found to be without vibronic features and are situated in between the toluene (less polar) and the dilute solutions in THF (more polar).

Interestingly, the emission spectra of solid-film compounds **3** and **4** containing methoxy groups in the peripheral phenyl moieties exhibit an additional broad and structure less band at larger wavelengths reported hereafter as band type II (350-600 nm, Figure 6). While the phosphorescence band appears at the same region (Figure S2), the band type II cannot be due to TADF emission, as this should then appear at higher energies corresponding to singlet emission. Additionally, the band type II is absent in the case of compounds **1** and **2**, despite the presence of the phosphorescence emission at the same region. We deduce consequently that the emission band type II is of excimeric origin. The appearance of this band only in the presence of the peripheral methoxy groups is consistent with the idea that methoxy groups can strengthen the intermolecular interaction by means of hydrogen bonds[28,30,46], which is expected to help excimer formation[57].

Fluorescence quantum yields (Φ_F) of dilute solutions in THF, toluene and of the solid films of the compounds are given in Table 3. Fluorescence spectra show globally low quantum yields, which seems to correlate with the very small oscillator strengths of the $S_0 \rightarrow S_1$ CT transitions. The films of compounds **1** and **2** exhibited considerably higher emission quantum yields than the corresponding dilute solutions. Φ_F values of the films of compounds **3**, **4** were found to be considerably lower than those of the films of compounds **1**, **2** and comparable to those of their dilute solutions. This seems coherent with the enhanced intermolecular interactions in the solid films of these compounds, in turn due to the establishment of hydrogen bonds by means of the peripheral methoxy groups, some dynamical PL quenching can be expected[58].

The triplet energies (E_T) of the compounds were calculated to be of ca. 2.66 eV. The calculated values were found to be in good agreement with the experimental values of 2.86 eV which were taken from phosphorescence spectra of the dilute solutions of the studied compounds (Figure S2). ΔE_{ST} values of 0.51-0.52 eV for the *ortho*-methoxy substituted compounds (**1**, **3**) and 0.60 for the *meta*-methoxy substituted compounds (**2**, **4**) were found in solid films and in toluene, thus suggesting more efficient TADF in the case of *ortho*-methoxy substituted compounds.

Fluorescence decay curves of the dilute THF solutions of compounds **1**–**4** demonstrated single exponential decay profiles. Fluorescence life times (τ) of the dilute solutions of *o*-methoxytriphenylamine-based compounds (**1** and **3**) were found to be longer than those of the corresponding *m*-methoxytriphenylamine-based counterparts (**2** and **4**).

Table 3. Optical and photophysical properties of the dilute solutions and neat films of compounds **1**–**4**.

Compound	Solution									Film	
	in THF							in toluene			
	λ_{abs}^{max}, nm	λ_{FL}^{max} at 300 K/77 K, nm	Φ_{FL} %	τ, ns	χ^2	E_T	E_T *theor*	λ_{FL}^{max}, nm	Φ_{FL}, %	λ_{FL}^{max}, nm	Φ_{FL}, %
1	268, 309	406/368	8	5.31	1.092	2.86	2.66	381	9	387	32
2	269, 309	370/358	21	1.91	1.045	2.86	2.65	364	8	367	29
3	270, 310	404/367	7.5	7.03	1.106	2.86	2.66	379	11	386	11
4	271, 310	370/358	15	1.87	1.140	2.86	2.65	364	8	365	5

λ_{abs}^{max} – absorption maximum.

λ_{F}^{max} – emission maximum (λ_{ex} = 310 nm).

Φ_F – quantum yield.

τ – fluorescence life time measured at λ_{F}^{max} (λ_{ex} = 310 nm).

χ^2 – least squares fitting of experimental fluorescence decay data.

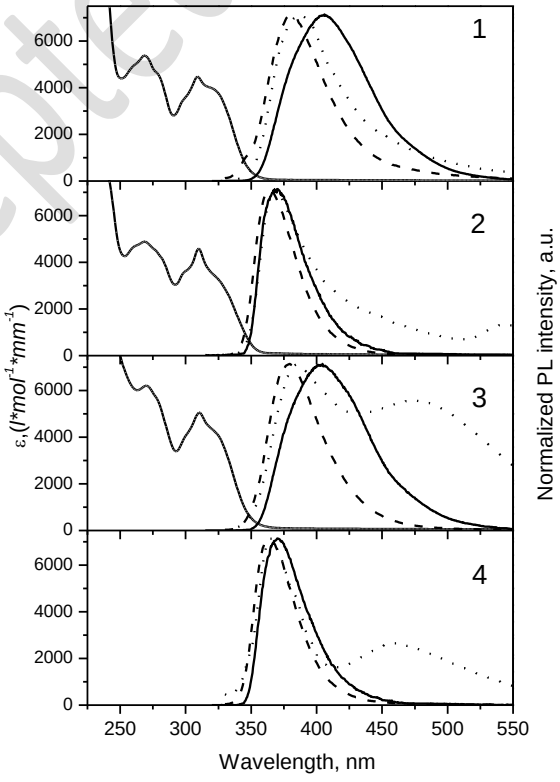

Figure 6. Absorption and fluorescence spectra of compounds **1**–**4** at 300 K (solid line – absorption and fluorescence spectra of dilute solutions in THF, dashed line – fluorescence of dilute solutions in toluene, dotted line – fluorescence of solid films)

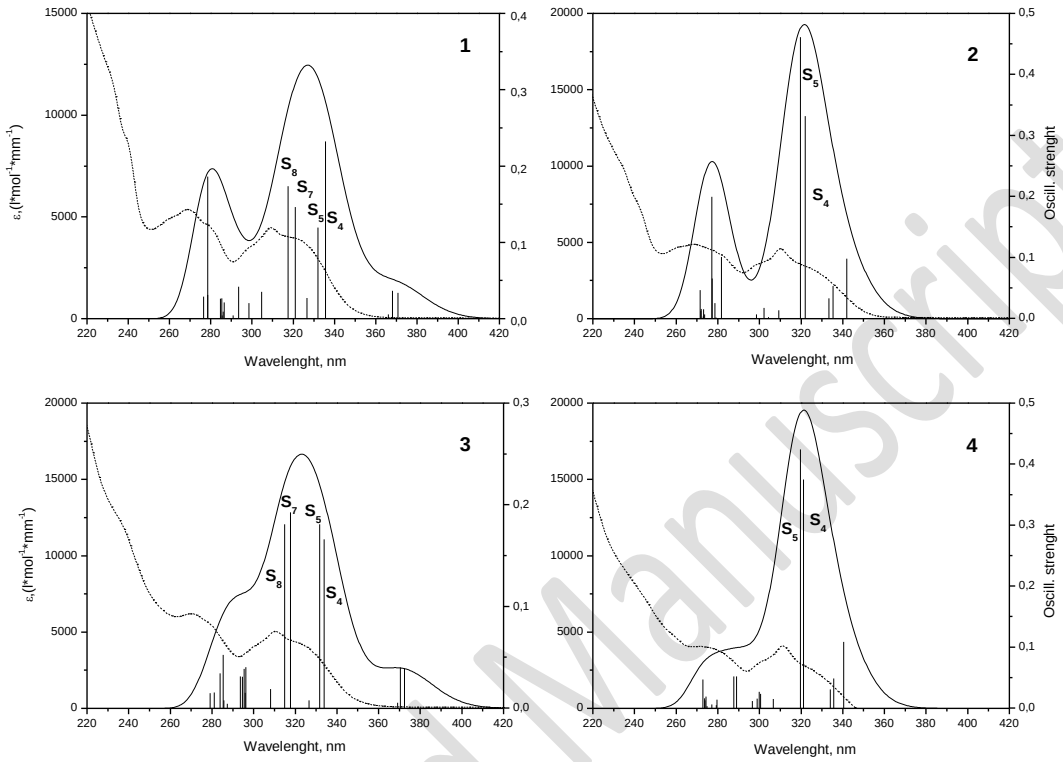

Figure 7. Experimental absorption spectra of 10^{-5} M THF solutions of compounds **1**–**4** and theoretical ones (solid curves) obtained by means of TDB3LYP/6-31G(d,p) calculations ‘‘in gas phase’’.

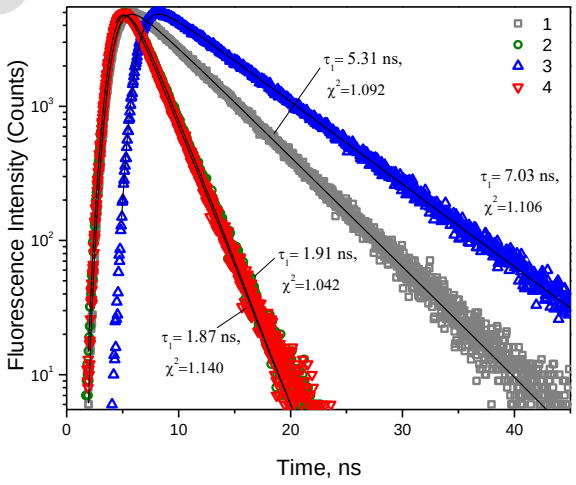

Figure 8. Fluorescence transients of dilute (10^{-5} M) solutions in THF of derivatives **1**–**4**. Fluorescence lifetimes (τ) and least squares fitting of experimental data (χ^2) are indicated.

3.6. Charge Transporting Properties

Time of flight measurements were used for the estimation of charge-transporting properties of the compounds. Figure 9 shows electric field dependencies of hole and electron drift mobilities (μ) for the layers of compounds **1**–**4**. All the compounds showed the linear dependencies of charge mobilities on the square root of the electric field. Compounds **1**–**3** showed bipolar charge-transporting properties with the comparable mobilities of holes and electrons. The charge carrier mobility values are summarized in Table 4. Comparison of the charge-transporting properties of the synthesized compounds revealed the dependence of charge mobilities on the position of methoxy groups in triphenylamine moiety. Compounds **2** and **4** with *meta*-methoxy substituted triphenylamine core showed higher charge mobilities than the corresponding counterparts with *ortho*-substituted central unit (**1** and **3**). The highest charge mobilities were observed for the layer of compound **2** which showed hole mobility of 1.4×10^{-3} cm^2/Vs and electron mobility of 8.8×10^{-4} cm^2/Vs at an electric field of 6.4×10^5 V/cm.

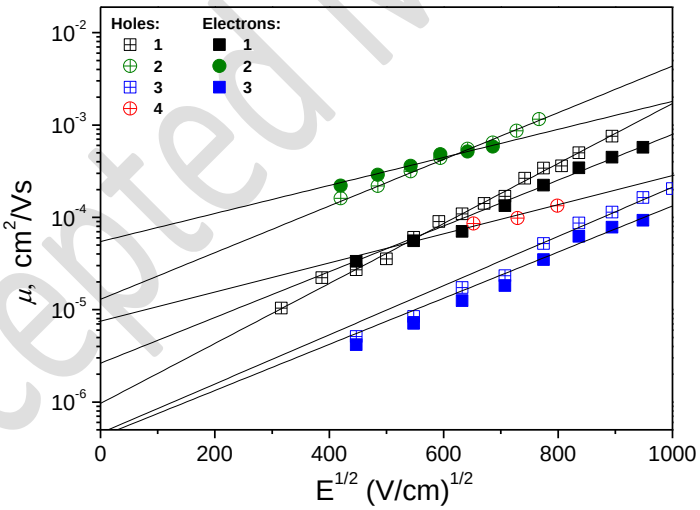

Figure 9. Electric field dependencies of hole and electron drift mobilities for the layers of compounds **1**–**4** at room temperature. The samples for the measurements were prepared by vacuum deposition.

In order to obtain more insight on the charge-transport properties of these compounds, we rely on Marcus theory, in which the rate-constant of hole-transfer between two adjacent molecules of amorphous materials can be calculated by means of the following equation:

$$k_{HT} = \frac{4\pi^2}{h}\frac{1}{\sqrt{4\pi\lambda k_B T}}t^2 exp\left[\frac{-(\Delta G^o+\lambda)^2}{4k_B\lambda T}\right] \quad (2)$$

In this equation *t* is the electronic coupling between two adjacent molecules, ΔG^0 is the reaction free energy, λ is the reorganization energy. This last parameter contains contributions from the medium polarization energy (λ_s), and from the energetic effort due to the intra-molecular geometric relaxations related to the charge transfer between two adjacent molecules (λ_i). The intra-molecular geometric relaxations (λ_i) correspond to the hole- and electron transports for each compound are given in Table 4.

Table 4. Time of flight hole and electron mobility parameters of the layers of compounds **1**–**4**. The intramolecular reorganization energies for hole and electron transport calculated at the B3LYP/6-31G(d,p) level are also shown.

Compound	μ_{h0}, cm^2/Vs	μ_h, cm^2/Vs	μ_{e0}, cm^2/Vs	μ_e, cm^2/Vs	λ_i^h, eV	λ_i^e, eV
1	9.4×10^{-7}	3.9×10^{-4}	2.6×10^{-6}	2.5×10^{-4}	0.245	0.100
2	1.3×10^{-5}	1.4×10^{-3}	5.2×10^{-5}	8.8×10^{-4}	0.153	0.099
3	4.4×10^{-7}	6.5×10^{-5}	4.0×10^{-7}	4.2×10^{-5}	0.243	0.107
4	5.5×10^{-6}	1.4×10^{-4}	-	-	0.165	0.103

Hole and electron mobility values at electric field of 6.4×10^5 V/cm.

The results shown in Table 4 indicate larger reorganization energies for hole transport than for electron transport, suggesting that, based on this factor only, the hole transport should be slightly inferior as compared to the electron transport. This seems consistent with the smaller μ_{h0} values for holes than for electrons. Although experimentally hole and electron transports are similar, electron transport is fractionally lower. This observation suggests that the intrinsic properties in these materials cannot account for the trends in the charge transfer, which mostly seems to depend on the disorder phenomena. The larger energy disorder for electron transport (larger LUMO energy distribution) as compared to holes seems to be due to the easier intermolecular interactions, hence geometrical deformations, between the peripheral acceptor moieties as compared to the interaction between the central and sterically hindered TPA moieties. However, the polaronic type transport depending on the intrinsic properties of these molecules seems to be not negligible, as similar trends are found for μ_{h0} and μ_h values, both being larger for compounds **2** and **4** as compared to **1** and **3**. Note that the larger μ_{h0} values for **2** and **4** by roughly 2 orders as compared to **1** and **3** may be due to the smaller λ_i^h values in the former case

(0.153-0.165 eV as compared to 0.243-0.245 eV respectively, Table 4). However, differences in HOMO-HOMO electronic couplings might also play, as steric hindrance around N atom in the TPA moieties seems to be larger in **1** and **3** (hence smaller electronic couplings) as compared to **2** and **4**.

As an example, the current transient curves of holes and electrons for compound **1** at different electric fields are presented in Figure 10. Clear transit time for holes or electrons were not seen in the linear scales due to the dispersive charge transport, however, they were well recognized in log-log scales for both holes and electrons. Current transient curves of the other studied compounds showed similar behaviors.

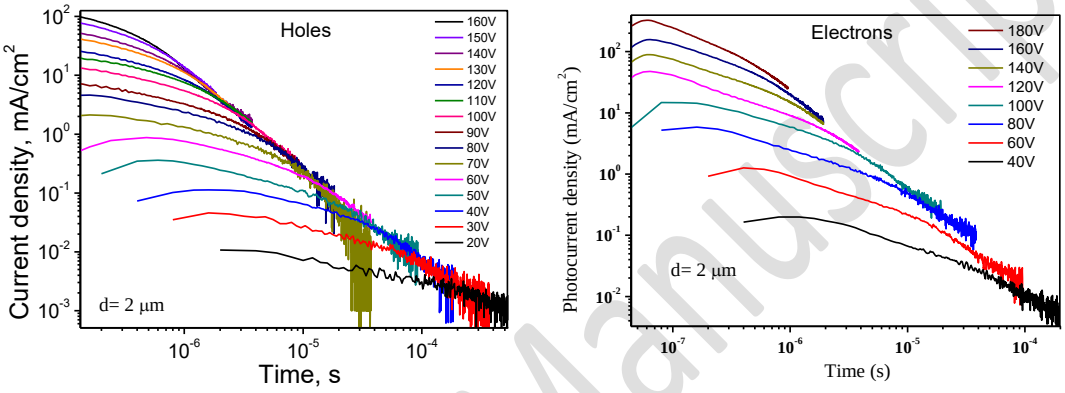

Figure 10. Current transient pulses of holes and electrons for the layer of **1** at the different electric fields at room temperature.

3.7. Exciplex-Forming Properties of Compounds 1–4

To study exciplex-forming properties of compounds **1–4,** the layers of the molecular mixtures of the donor compounds **1–4** and the acceptor compounds 4,7-diphenyl-1,10-phenanthroline (Bphen) or 2,9-dimethyl-4,7-diphenyl-1,10-phenanthroline (BCP) were prepared. The shifts of fluorescence (FL) spectra of the layers of the molecular mixtures to the long-wavelength region compared with the photoluminescence spectra of compounds **1–4**, BPhen and BCP, which peaks are in the near ultraviolet region, were observed (Figure 11a, b). The fluorescence spectra of these molecular mixtures are characterized by broad emission bands with the peaks in range from 427 to 485 nm. The similar shifts of fluorescence spectra were previously observed for the donor-acceptor molecular systems capable of the exciplex formation[14,17,19]. We assumed that fluorescence spectra of the mixtures **1–4**:BPhen(BCP) are influenced by the exciplex formation. To confirm this assumption, we recorded the FL life times and the FL quantum efficiencies of the molecular mixtures (Figure 11c, d, Table 5). The FL decay curves were well fitted (χ^2 were not higher then 1.3) by the double exponential law $A+B1\exp(-t/\tau_1)+B2\exp(-t/\tau_2)$. The life times ($\tau_1$, τ_2) of the layers of the mixtures **1–4**:BPhen (BCP) are given in Table 5. Both τ_1 and τ_2 of the

mixtures were longer than the FL life times of the solid samples of pure **1–4,** BPhen or BCP. The increased FL life times of the mixtures can be explained by the formation of intermolecular charge transfer (CT) complexes between the molecules of **1–4** and BPhen(BCP) and, as a result, formation of the exciplexes. The shorter component τ_1 is apparently associated with the singlet exciplex emission, and the longer component τ_2 is related to the TADF effect of exciplexes due to the reverse intersystem crossing (RISC) mechanism from singlet to triplet state[19,36]. The life times (τ_1, τ_2) of exciplexes based on *o*-methoxytriphenylamine-based compounds (**1**, **3**) were found to be longer than those observed for exciplexes based on the *m*-methoxytriphenylamine-based counterparts (**2**, **4**). The peaks of exciplex emission for the mixtures **2**(**4**):BPhen(BCP) were blue-shifted compared to those observed for the mixtures **1**(**3**):BPhen(BCP), which is due to the lower HOMOs of **2** and **4**, hence their larger HOMO(**2**, **4**)-LUMO(BPhen(BCP)) gap as compared to **1** and **3**. The shoulders at ca. 350-360 nm belong to fluorescence emission of the studied compounds.

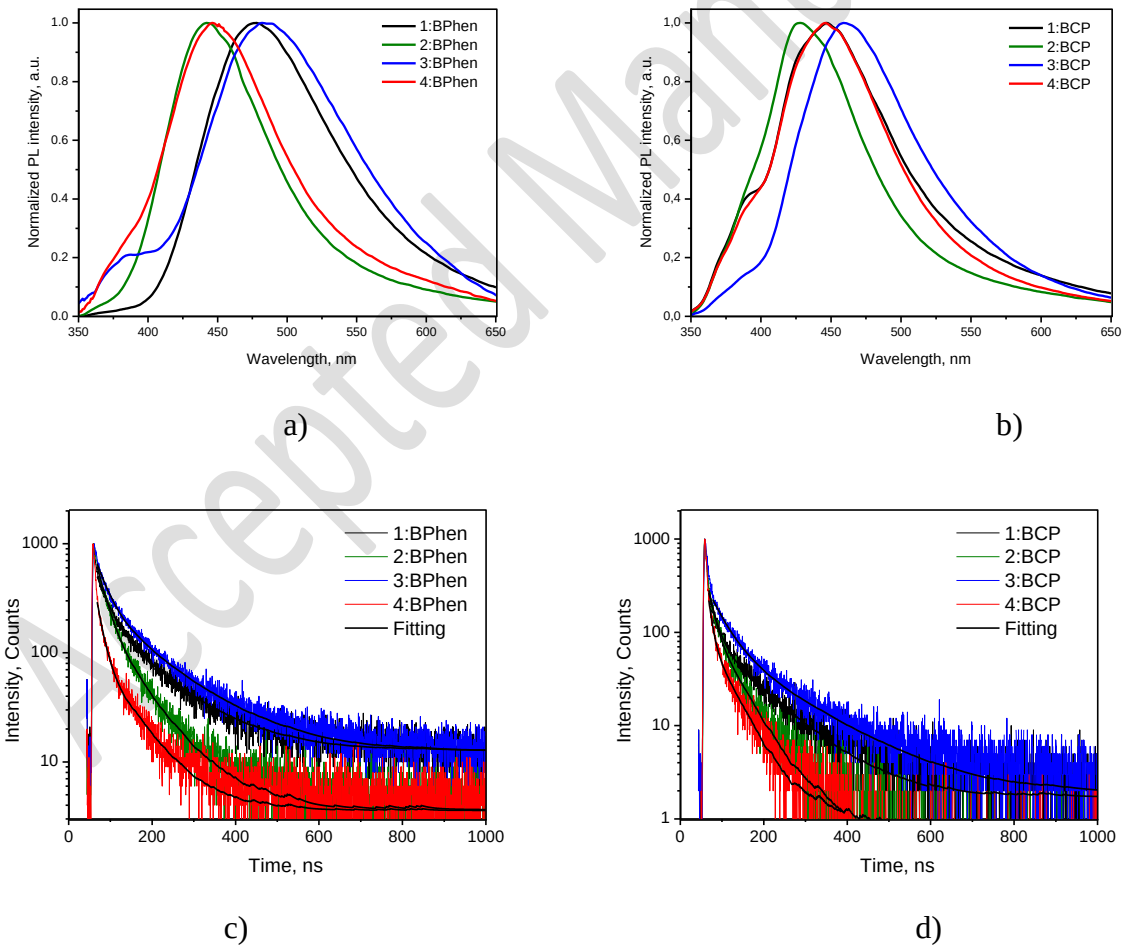

Figure 11. Fluorescence spectra and transients FL curves of the layers of the mixtures of compounds **1–4** with **BPhen** or **BCP**.

In general, the radiative electronic transition from the LUMO of an acceptor to the HOMO of a donor results in exciplex emission with the emission maximum, described by the following equation[14]:

$$hv_{ex}^{max} \simeq I_P^D - E_A^A - E_C \qquad (3)$$

where I_P^D is the ionization potential of the donor, E_A^A is the electron affinity of the acceptor, and E_C is the electron–hole Coulombic attraction energy. The emission maximum of 440 nm (2.8 eV) of the exciplex **2**:BPhen was found. Interestingly the application of Eq. 3 results in a value of $hv_{ex}^{max} \simeq 2.76$ eV, by using the I_P (5.41 eV) of **2**, the E_A (3 eV) of BPhen, and a typical value of -0.35 eV for the e-h binding energy in organic materials, thus showing good agreement with the experimental value. Similar behaviors were observed for all the studied exciplexes based on compounds **1–4**. The reason of the differences between the calculated and measured values could be due the bending of HOMO, LUMO levels at the donor-acceptor interface[59] and to the lack of exact e-h binding energies.

Table 5. Fluorescence quantum yields and photoluminescence transients of the layers containing mixtures of compounds **1–4** and Bphen or BCP.

Mixture	λ_{FL}^{max}, nm	Φ_{FL}, %	τ, ns	χ^2
1:BPhen	475	13.64	28.3 (40.2%), 119.26 (59.8%)	1.121
2:BPhen	442	12.62	23.92 (63%), 82.33 (37%)	1.169
3:BPhen	483	12.64	28.06 (40%), 133.87 (60%)	1.129
4:BPhen	447	15.71	15.47 (55%), 72.45 (45%)	1.182
1:BCP	447	-	17.82 (47.0%), 101.55 (53%)	1.097
2: BCP	427	12.68	13.64 (45%), 50.38 (55%)	1.045
3: BCP	460	-	36.80 (52%), 149.98 (60%)	1.198
4: BCP	447	23.96	8.53 (46%), 43.8 (54%)	1.072

3.8. White Organic Light-Emitting Diodes

To fabricate white organic light-emitting diodes (WOLEDs), we combined the blue **2**:BPhen and green 4,4′,4″-tris[3-methylphenyl(phenyl)amino]triphenylamine (m-MTDATA):Bphen exciplexes as the two different emitters. The device of the following structure was fabricated: indium tin oxide (ITO)/m-MTDATA(30 nm)/**2**:BPhen(25 nm)/BPhen(25 nm)/Ca(10 nm)/Al(60 nm) (Figure 12a). In the following discussion this devices will be referred as WhiteD. In this device the blue **2**:BPhen exciplex was formed in the emitting layer (EML) and green m-MTDATA:Bphen exciplex was formed on an interface between the m-MTDATA hole-transporting layer (HTL) and the EML. The BPhen layer was used as an electron-transporting layer (ETL). The EML contained 70 wt% of **2** and 30 wt% of BPhen. According to HOMO and LUMO levels of the materials used, it should be no difficulties for the injection of holes and electrons from the ITO anode and from the Ca cathode to EML (Figure 12a).

The electroluminescence (EL) spectra of the WhiteD recorded at the different applied voltages are shown in Figure 12b. The EL spectrum observed at 5 V is characterized by broad emission band with the peak at 527 nm and the shoulders in the blue and red regions. The position of the shoulder in the blue region at 430 nm is close to the position the FL band of blue exciplex **2**:BPhen (Figure 11a). This shoulder cannot be attributed to the emission of pure m-MTDATA because of the strong energy barrier for electrons which appears due to the difference of the LUMO energies of m-MTDATA and BPhen. The emission band in the electroluminescence spectrum of WhiteD peaking at 527 nm is attributed to the green m-MTDATA:Bphen exciplex[36]. The shoulder observed in the red region at 620 nm, which was not observed in the FL spectra of pure **2** and of the mixture **2**:BPhen, apparently originates from the electroplex of the layer of **2**:BPhen that is associated with the exciplex emission[14]. The EL spectrum of the WhiteD does not contain emission from the pure m-MTDATA, **2** and Bphen which indicates that holes and electrons radiatively recombine on the exciplex forming sites in WhiteD. Overlapping emission spectra of the two exciplexes resulted in the shift of EL peak of WhiteD to higher energy region with increasing applied voltage (Figure 12b). Commission Internationale de l'Eclairage (CIE 1931 and CIE 1976) chromaticity coordinates (x, y) and (u'; v') of the WhiteD were found to be from (0.286, 0.378) to (0.24, 0.29) and from (0.164, 0.489) to (0.16, 0.435), respectively, corresponding to cold-white color with color temperatures higher than 6500 K (Figure 13). The CIE chromaticity coordinates of the WhiteD corresponded to white color at all the external voltages used.

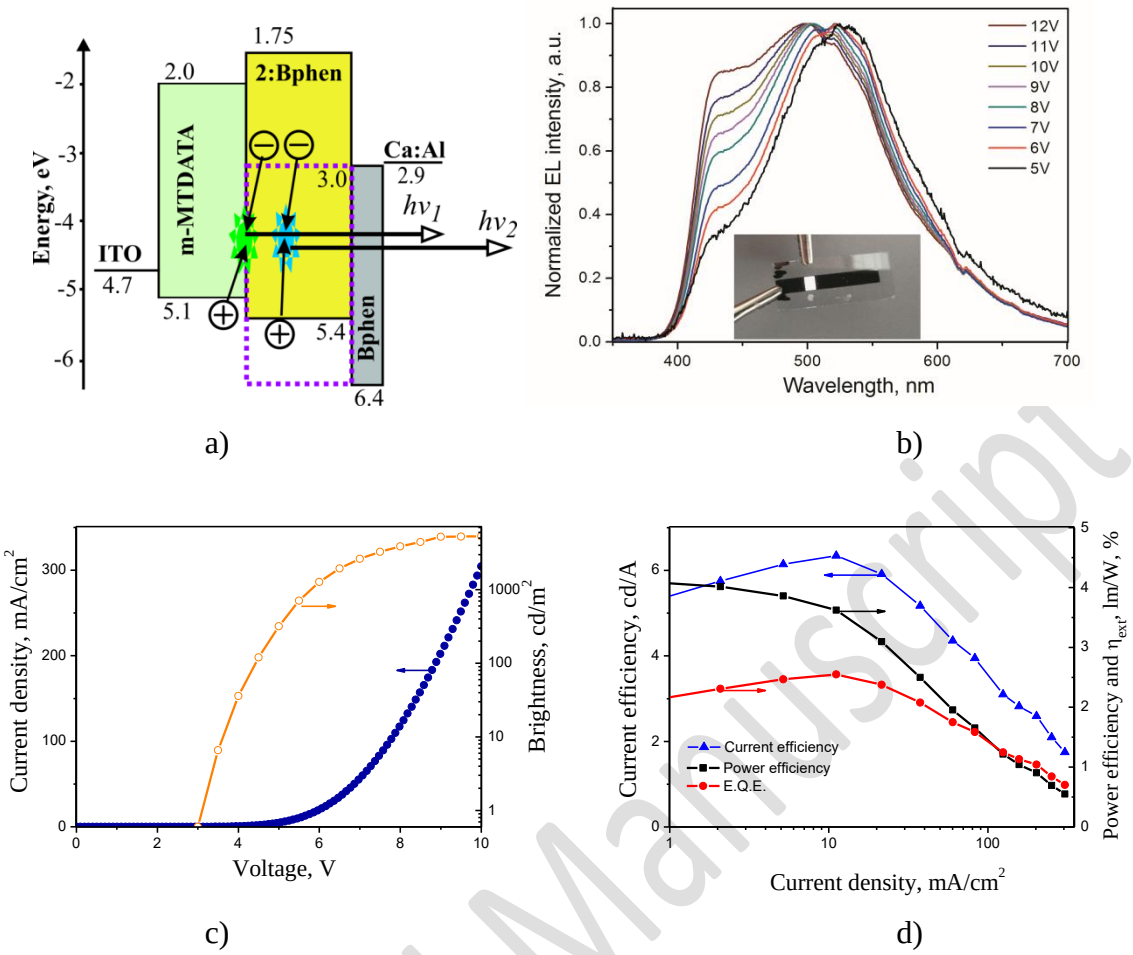

Figure 12. Energy-band diagram (a) and electroluminescence spectra (b) of WhiteD. Current density–voltage– luminance characteristics (c) and current efficiency−current density−power efficiency−external quantum efficiency characteristics (d) of WhiteD.

The energy-band diagram of the device WhiteD is shown in Figure 12a. Injected holes from ITO under external applied voltage can drift across the HTL and **2** due to the concordance of HOMO of m-MTDATA and HOMO of **2**. Holes then are blocked on the interface EML/ETL due to the energy barrier. According to the LUMO of **2**, injected electrons from the Ca cathode to the ETL can drift through the ETL as well as through the included BPhen EML and reach the HTL/EML interface without any energy barriers. A difference between HOMO of m-MTDATA and that of **2** produce a shallow energy barrier for holes, therefore, holes and electrons radiatively recombine on the HTL/EML interface emitting the green m-MTDATA:Bphen exciplex light in WhiteD. Injected holes into the EML radiatively recombine with the electrons thus emitting the blue **2**:BPhen exciplex light near the HTL/EML interface since the hole mobility of **2** (Figure 9) is lower than the electron mobility of BPhen[60]. The increase of the intensity of the shoulder in the blue region (at 430 nm) of the EL spectrum of WhiteD compared to that of the peak at 527 nm

with the increase of the applied external voltage (Figure 12b) is apparently due to the deeper hole penetration and the spreading of the recombination zone through the entire EML.

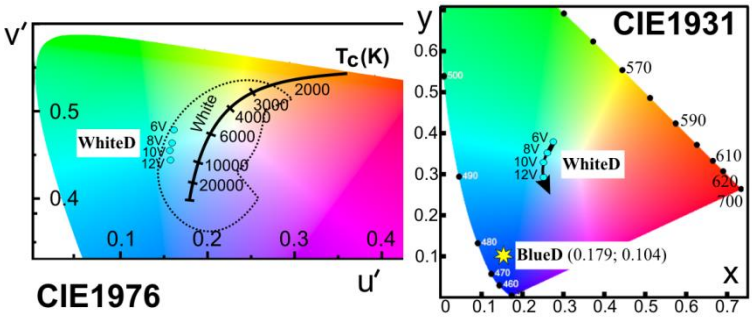

Figure 13. CIE1976 and CIE1931 diagrams for the devices WhiteD and BlueD.

The current density–voltage– luminance characteristics of WhiteD are shown in Figure 12c. The turn on voltage of 3.6V was observed at 10 cd/m^2 which are similar to the values of well-constructed OLEDs[61]. The maximum brightness of WhiteD reached 5300 cd/m^2 at 10 V. Figure 12d shows the current (η_c), power (η_p), and external quantum efficiencies as the functions of luminance for WhiteD. The values of maxima of η_c, η_p, and η_{ext} were observed at 6.34 cd/A, 4.09 lm/W, and 2.55%, respectively. The efficiencies of WhiteD are not very good compared with those of OLEDs with the optimized structures with one formed exciplex[7,36]. The efficiencies of the exciplex-based OLEDs can be improved by the optimization of charge carrier balance between the two exciplexes[36].

3.9. Blue Organic Light-Emitting Diodes

We fabricated blue OLED based on the blue **2**:BPhen exciplex as an emitter. The structure of the device was ITO/m-MTDATA(30 nm)/**2**(8 nm)/**2**:BPhen(25 nm)/BPhen(25 nm)/Ca(10 nm)/Al(60 nm) (Figure 14a). In the further discussion this device will be referred as BlueD. In this device, the HTL (m-MTDATA), EML (**2**:BPhen), and ETE (BPhen) were the same as in WhiteD. In BlueD compound **2** was used as the electron blocking material. The electron blocking layer (EBL) protected the HTL from electrons and the green m-MTDATA:Bphen exciplex could not be formed. Owing to the HOMO energy and hole-transporting properties of compound **2**, holes can be easily injected into the EML of BlueD. Therefore, holes and electrons radiatively recombine in EML emitting the blue **2**:BPhen exciplex light. The EL spectra of BlueD are plotted in Figure 14b. No substantial differences in the EL spectra recoded at the different applied voltages were observed. No emission from the green m-MTDATA:BPhen exciplex was recorded. This observation confirms good electron-blocking properties of compound **2**. We note that EL spectra of BlueD (Figure 14b) are very similar to the FL spectra of the mixture **2**:BPhen

(Figure 11a) and are not similar to FL spectra of pure **2** or BPhen (Figure 6). Therefore, the EL spectra of BlueD were characterized by blue exciplex emission while using **2**:BPhen as the emitter the deepest blue TADF emission reported so far was observed with the EL maximum at 428 nm and with the CIE 1931 chromaticity coordinates of (0.179; 0.104). Such CIE 1931 coordinates (0.179; 0.104) of the EL of the BlueD were close to the National Television System Committee (NTSC) blue color standard of (0.14, 0.08)[62].

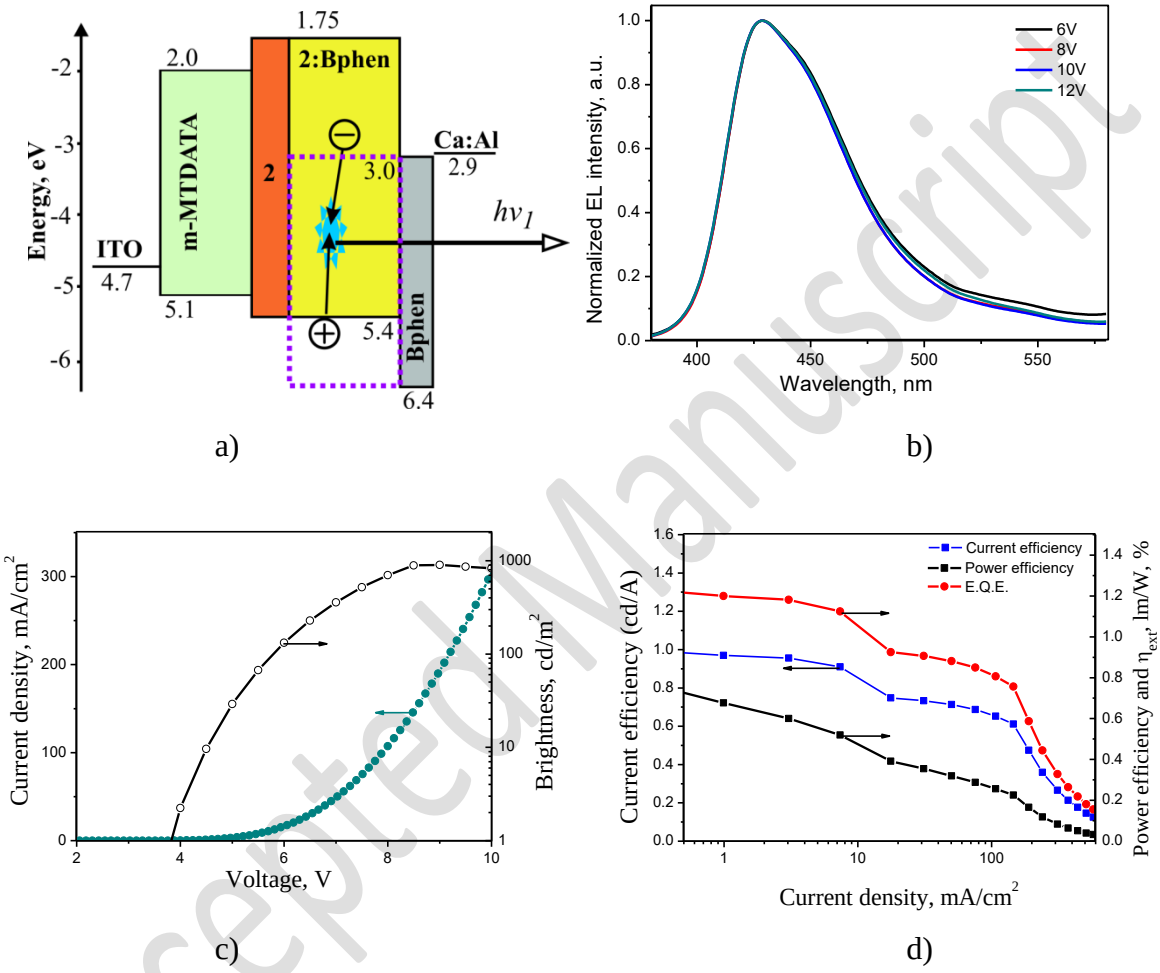

Figure 14. A energy-band diagram (a) and electroluminescence spectra (b) of BlueD. Current density–voltage–luminance characteristics (c) and current efficiency−current density−power efficiency−external quantum efficiency characteristics (d) of BlueD.

Figure 14c shows the current density–voltage–luminance characteristics. For the BlueD, the turn on voltage of 4.5V (it was taken at 10 cd/m^2) was found to be higher than that observed for WhiteD. The increase of the turn on voltage of BlueD was apparently caused by the effect of the additional layer in the structure of the device. The maximum brightness of 900 cd/m^2 was recorded at 9 V for BlueD. Such brightness is comparable with that reported earlier for deep blue fluorescent OLEDs[63]. The plots of η_c, η_p, and η_{ext} as functions of current density for BlueD are shown in Figure 14d. The values of maxima of η_c, η_p, and η_{ext} were observed at 1 cd/A, 0.75

lm/W, and 1.2%, respectively. The additional approaches, such as the optimization of the concentration of BPhen in its mixture with **2** and the optimization of the thicknesses of the layers of the devices, can be used to improve the performance of BlueD.

Conclusions

We synthesized and characterized new derivatives of methoxytriphenylamine having phenylfluorenyl or methoxyphenylfluorenyl moieties as substituents and studied their thermal, optical photophysical and photoelectrical properties. The synthesized triphenylamine derivatives were found to constitute glass-forming materials with glass transition temperatures being in the range of 151-165 °C as characterized by differential scanning calorimetry. Electron photoemission spectra of the solid samples of the materials revealed ionization potentials of 5.25-5.41 eV. Most of the synthesized compounds showed bipolar charge transport. The highest charge mobilities were observed for the layer of tris[3-methoxy-4-(9-phenyl-9-fluorenyl)phenyl]amine which showed hole mobility of 1.4×10^{-3} cm^2/Vs and electron mobility of 8.8×10^{-4} cm^2/Vs at an electric field of 6.4×10^5 V/cm. The theoretical results suggested similar geometries of the compounds, similar HOMO and LUMO distributions, and similar absorption and fluorescence spectra. The impact of the methoxy substituents in *meta*- or *ortho* positions in TPA was found to be important with respect to the HOMO energy and ionization potentials, being roughly 0.3 eV smaller in the case of *ortho* isomers. As for the methoxy substituents at the peripheral phenyl groups, a negative impact was found, translated in reduced charge transport and in reduced fluorescence quantum yield in solid films. Exciplex-forming properties of the synthesized compounds with known acceptors were discovered while deep blue TADF emitters were found. Possible applications of the exciplex emitters for either cold-white with the CIE 1931 chromaticity coordinates of (0.24, 0.29) at 12 V or deep-blue with the CIE 1931 chromaticity coordinates of (0.179; 0.104) OLEDs were proposed. The maximum brightness of the cold-white OLED reached 5300 cd/m^2 at 10 V while the values of maxima of current, power, and external quantum efficiencies were observed at 6.34 cd/A, 4.09 lm/W, and 2.55%, respectively.

Acknowledgement

This research was supported by H2020-ICT-2014/H2020-ICT-2014-1 project PHEBE (grant agreement No 641725).

References

(1) Reineke, S. Complementary LED Technologies. *Nat. Mater*. **2015**, *14*, 459−462.

(2) Fyfe, D. LED Technology. Organic Displays Come of Age. *Nature Photon.* **2009**, *3*, 453−455.

(3) Leo, K. Organic Light-Emitting Diodes. Efficient and Flexible Solution. *Nature Photon.* **2011**, *5*, 716−718.

(4) Aizawa, N.; Pu, Y.-J.; Watanabe, M.; Chiba, T.; Ideta, K.; Toyota, N.; Igarashi, M.; Suzuri, Y.; Sasabe, H.; Kido, J. Solution-Processed Multilayer Small-Molecule Light-Emitting Devices with High-Efficiency White-Light Emission. *Nat. Commun.* **2014**, DOI: 10.1038/ncomms6756

(5) Tsutsui, T. Progress in Electroluminescent Devices Using Molecular Thin Films. *MRS Bulletil*. **1997**, 39−45.

(6) Adachi, C.; Baldo, M. A.; Thompson, M. E.; Forrest, S. R. Nearly 100% Internal Phosphorescence Efficiency in an Organic Light-Emitting Device. *J. Appl. Phys.* **2001**, *90*, 5048–5051.

(7) Kido, J.; Kimura, M.; Nagai, K. Multilayer White Light-Emitting Organic Electroluminescent Device. *Science*. **1995**, *267*, 1332−1334.

(8) Bucinskas, A.; Volyniuk, D.; Danyliv, Y.; Grazulevicius, J. V.; Baryshnikov, G.; Minaev, B.; Ivaniuk, K.; Cherpak, V.; Stakhira, P. N-Annelated Perylenes as Effective Green Emitters for OLEDs. *RSC Adv*. **2015**, *5*, 78150–78159.

(9) Wang, Z. B.; Helander, M. G.; Qiu, J.; Puzzo, D. P.; Greiner, M. T.; Hudson, Z. M.; Wang, S.; Liu, Z. W.; Lu, Z. H. Unlocking the Full Potential of Organic Light-Emitting Diodes on Flexible Plastic. *Nature Photon.* **2011**, *5*, 753−757.

(10) Reineke, S.; Lindner, F.; Schwartz, G.; Seidler, N.; Walzer, K.; Lussem, B.; Leo, K. White Organic Light-Emitting Diodes with Fluorescent Tube Efficiency. *Nature*. **2009**, *459*, 234−239.

(11) Sun, Y.; Giebink, N.C.; Kanno, H.; Ma, B.; Thompson, M.E.; Forrest, S.R. Management of Singlet and Triplet Excitons for Efficient White Organic Light-Emitting Devices. *Nature*. **2006**, *440*, 908−912.

(12) Uoyama, H.; Goushi, K.; Shizu, K.; Nomura, H.; Adachi, C. Highly Efficient Organic Light-Emitting Diodes from Delayed Fluorescence. *Nature*. **2012**, *492*, 234−238.

(13) Jankus, V.; Data, P.; Graves, D.; McGuinness, C.; Santos, J.; Bryce, M. R.; Dias, F. B.; Monkman, A. P. Highly Efficient TADF OLEDs: How The Emitter−Host Interaction Controls Both the Excited State Species and Electrical Properties of the Devices to Achieve Near 100% Triplet Harvesting and High Efficiency. *Adv. Funct. Mater.* **2014**, *24*, 6178−6186.

(14) Kalinowski, J. Excimers and Exciplexes in Organic Electroluminescence. *Mater. Sci.-Pol.* **2009**, *27*, 735−756.

(15) Cherpak, V.; Stakhira, P.; Minaev, B.; Baryshnikov, G.; Stromylo, E.; Helzhynskyy, I.; Chapran, M.; Volyniuk, D.; Hotra, Z.; Dabuliene, A.; Tomkeviciene, A.; Voznyak, L.; Grazulevicius, J.V. Mixing of Phosphorescent and Exciplex Emission in Efficient Organic Electroluminescent Devices. *ACS Appl. Mater. Interfaces* **2015**, *7*, 1219−1225

(16) Cherpak, V.; Stakhira, P.; Minaev, B.; Baryshnikov, G.; Stromylo, E.; Helzhynskyy, I.; Chapran, M.; Volyniuk, D.; Tomkute-Luksiene, D.; Malinauskas, T.; Getautis, V.; Tomkeviciene, A.; Simokaitiene, J.; Grazulevicius, J.V. Efficient "Warm-White" OLEDs Based on the Phosphorescent bis-Cyclometalated iridium(III) Complex. *J. Phys. Chem. C* **2014**, *118*, 11271−11278.

(17) Michaleviciute, A.; Gurskyte, E.; Volyniuk, D.Yu.; Cherpak, V.V.; Sini, G.; Stakhira, P.Y.; Grazulevicius, J.V. Star-Shaped Carbazole Derivatives for Bilayer White Organic Light-Emitting Diodes Combining Emission from Both Excitons and Exciplexes. *J. Phys. Chem. C* **2012**, *116*, 20769−20778

(18) Zhang, Q.; Li, B.; Huang, S.; Nomura, H.; Tanaka, H.; Adachi, C. Efficient Blue Organic Light-Emitting Diodes Employing Thermally Activated Delayed Fluorescence. *Nature Photon.* **2014**, *8*, 326-332.

(19) Zhang, T.; Zhao, B.; Chu, B.; Li, W.; Su, Z.; Wang, L.; Wang, J.; Jin, F.; Yan, X.; Gao, Y.; Wu, H.; Liu, C.; Lin, T.; Hou, F. Blue Exciplex Emission and its Role as a Host of Phosphorescent Emitter. *Org Electron*. **2015**, *24*, 1–6.

(20) Higuchi, T.; Nakanotani, H.; Adachi, C. High-Efficiency White Organic Light-Emitting Diodes Based on a Blue Thermally Activated Delayed Fluorescent Emitter Combined with Green and Red Fluorescent Emitters. *Adv. Mater.* **2015**, DOI: 10.1002/adma.201404967.

(21) Hung, W.Y.; Fang, G.C.; Lin, S.W.; Cheng, S.H.; Wong, K.T.; Kuo, T.Y.; Chou, P.T. The First Tandem, All-exciplex-based WOLED. *Sci. Rep.* **2014**, DOI: 10.1038/srep05161.

(22) Zhang, T.; Zhao, B.; Chu, B.; Li, W.; Su, Z.; Yan, X.; Liu, C.; Wu, H.; Gao, Y.; Jin. F.; Hou, F. Simple Structured Hybrid WOLEDs Based on Incomplete Energy Transfer Mechanism: from Blue Exciplex to Orange Dopant. *Sci. Rep.* **2015**, DOI: 10.1038/srep10234.

(23) Iwan, A.; Sek, D. Polymers with Triphenylamine Units: Photonic and Electroactive Materials. *Prog.Polym. Sci*. **2011**, *36*, 1277–1325.

(24) Tao, Y. T.; Yang, C. L.; Qin, J. G. Organic Host Materials for Phosphorescent Organic Light-Emitting Diodes. *Chem. Soc. Rev.* **2011**, *40*, 2943–2970.

(25) Singh, S. P.; Roy, M. S.; Thomas, K. R. J.; Balaiah, S.; Bhanuprakash, K.; Sharma, G. D. New Triphenylamine-Based Organic Dyes with Different Numbers of Anchoring Groups for Dye-Sensitized Solar Cells. *J. Phys. Chem. C.* **2012**, *116*, 5941–5950.

(26) Metri, N.; Sallenave, X.; Plesse, C.; Beouch, L.; Aubert, P. H.; Goubard, F.; Chevrot, C.; Sini, G.; Processable Star-Shaped Molecules with Triphenylamine Core as Hole-Transporting Materials: Experimental and Theoretical Approach. *J. Phys. Chem. C.* **2012**, *116*, 3765−3772.

(27) Zhao, Z. J.; Li, Z.F.; Lam, J. W. Y.; Maldonado, J. L.; Ramos-Ortiz, G.; Liu, Y.; Yuan, W. Z.; Xu, J. B.; Miao, Q.; Tang, B. Z. High Hole Mobility of 1,2-bis[4′-(diphenylamino)biphenyl-4-yl]-1,2-diphenylethene in Field Effect Transistor. *Chem. Commun.* **2011**, *47*, 6924–6926.

(28) Keruckas J., Lygaitis R., Simokaitiene J., Grazulevicius J.V., Jankauskas V., Sini G. Influence of Methoxy Groups on the Properties of 1,1-bis(4-aminophenyl)cyclohexane Based Arylamines: Experimental and Theoretical Approach. *J. Mater. Chem.* **2012**, *22*, 3015–3027.

(29) Gudeika, D.; Michaleviciute, A.; Grazulevicius, J.V.; Lygaitis, R.; Grigalevicius, S.; Jankauskas, V.; Miasojedovas, A.; Jursenas, S.; Sini, G. Structure Properties Relationship of Donor-Acceptor Derivatives of Triphenylamine and 1,8-Naphthalimide, *J. Phys. Chem. C*, **2012**, *116*, 14811–14819.

(30) Gudeika, D.; Grazulevicius, J.V.; Sini, G.; Bucinskas, A.; Jankauskas, V.; Miasojedovas, A.; Jursenas, S. New Derivatives of Triphenylamine and Naphthalimide as Ambipolar Organic Semiconductors: Experimental and theoretical approach, *Dyes Pigtm.* **2014**, *106*, 58–70.

(31) Shih, P.I.; Chien, C.H.; Wu, F.I.; Shu, C.F. A Novel Fluorene-Triphenylamine Hybrid That is a Highly Efficient Host Material for Blue-, Green-, and Red-Light-Emitting Electrophosphorescent Devices. *Adv. Funct. Mater*. **2007**, *17*, 3514–3520.

(32) Hou, X.-Y.; Cheng Li, T.; Yin, C.-R.; Xu, H.; Lin, J.; Hua, Y.-R.; Chen, D.-Y.; Xie, L.-H.; Huanga, W. Stable Hole-Transporting Molecular Glasses Based on Complicated 9,9-Diarylfluorenes (CDAFs). *Synth. Met.* **2009**, *159*, 1055–1060.

(33) Zhang, C.; Zhang, Y.J.; Xiang, W.Q.; Hu, B.; Ouyang, M.; Xu, Y.; Ma, C.A. The Construction of H-Shaped Fluorescent Materials Based on Building Blocks Consisting of Triphenylamine and Fluorene. *Chem. Lett.* **2010**, *39*, 520–521.

(34) Wang, D. ; Li, W. ; Chu, B. ; Su, Z.; Bi, D. Highly Efficient Green Organic Light-Emitting Diodes from Single Exciplex Emission. *Appl. Phys. Lett.* **2008**, *92*, 053304 1-3.

(35) Wang, D.; Li, W. L.; Su, Z. S.; Li, T. L.; Chu, B.; Bi, D. F.; Chen, L. L.; Su, W. M.; He, H. Broad Wavelength Modulating and Design of Organic White Diode Based on Lighting by Using Exciplex Emission from Mixed Acceptors. *Appl. Phys. Lett.* **2006**, *89*, 233511 1-3.

(36) Zhang, T.; Chu, B.; Li, W.; Su, Z.; Peng, Q.M.; Zhao, B.; Luo, Y.; Jin, F.; Yan, X.; Gao, Y.; Wu, H.; Zhang, F.; Fan, D.; Wang, J. Efficient Triplet Application in Exciplex Delayed-Fluorescence OLEDs Using a Reverse Intersystem Crossing Mechanism Based on a ΔES−T of around Zero. *ACS Appl Mater Interfaces*. **2014**, *6*, 11907−11914.

(37) Bushby, R. J.; McGill, D. R.; Ng, K. M.; Taylor, N. p-Doped High Spin Polymers. *J.Mater.Chem.* **1997**, *7*, 2343-2354

(38) Vajiravelu, S.; Lygaitis, R.; Grazulevicius, J. V.; Gaidelis, V.; Jankauskas, V.; Valiyaveettil, S. Effect of Substituents on the Electron Transport Properties of Bay Substituted Perylene Diimide Derivatives. *J. Mater. Chem.* **2009**, *19*, 4268–4275.

(39) El-Khouly, M. E.; Ju, D. K.; Kay, K.-Y.; D'Souza, F.; Fukuzumi, S. Supramolecular Tetrad of Subphthalocyanine–Triphenylamine–Zinc Porphyrin Coordinated to Fullerene as an "Antenna-Reaction-Center" Mimic: Formation of a Long-Lived Charge-Separated State in Nonpolar Solvent. *Chem. Eur. J.* **2010**, *16*, 6193–6202.

(40) Kono, S.; Sinananwanich, W.; Shibasaki, Y.; Ando, S.; Ueda, M. Synthesis of Hyperbranched Polymer with Degree of Branching of Approximately 100% by Polycondensation of 2-(4-Phenoxyphenoxy)fluorenone. *Polym. J.* **2007**, *39*, 1150–1156.

(41) Zhan, X.; Risko, C.; Amy, F.; Chan, C.; Zhao, W.; Barlow, S.; Kahn, A.; Bredas, J.-L.; Marder, S.R. Electron Affinities of 1,1-diaryl-2,3,4,5-tetraphenyisiloles: Direct Measurements and Comparison with Experimental and Theoretical Estimates. *J. Am. Chem. Soc.* **2005**, *127*, 9021–9029.

(42) Qiao, Y.; Wei, Z.; Risko, C.; Li, H.; Bredas, J.-L.; Xu, W.; Zhu, D. Synthesis, Experimental and Theoretical Characterization, and Field-Effect Transistor Properties of a New Class of Dibenzothiophene Derivatives: From Linear to Cyclic Architectures. *J. Mater. Chem*. **2012**, *22*, 1313–1325.

(43) Kaafarani, B.R.; El-Ballouli, A.O.; Trattnig, R.; Fonari, A.; Sax, S.; Wex, B.; Risko, C.; Khnayze, R.S.; Barlow, S.; Patra, D.; Timofeeva, T.V.; List, E.J.W.; Bredas, J.L.; Marder, S.R. Bis(carbazolyl) Derivatives of Pyrene and Tetrahydropyrene: Synthesis, Structures, Optical Properties, Electrochemistry, and Electroluminescence. *J. Mater. Chem. C* **2013**, *1*, 1638–1650.

(44) Kukhta, N.A.; Volyniuk, D.; Peciulyte, L.; Ostrauskaite, J.; Juska, G.; Grazulevicius, J.V. Structure-Property Relationships of Star-Shaped Blue-Emitting Charge-Transporting 1,3,5-Triphenylbenzene Derivatives. *Dyes Pigm* **2015**, *117*, 122-132.

(45) Borsenberger, P. M.; Weiss, D. S. Organic Photoreceptors for Xerography. Marcel Dekker: New York, 1998.

(46) Mimaite, V.; Grazulevicius, J.V.; Laurinaviciute, R.; Volyniuk, D.; Jankauskas, V.; Sini, G. Can Hydrogen Bonds Improve the Hole-Mobility in Amorphous Organic Semiconductors? Experimental and Theoretical Insights. *J. Mater. Chem. C*, **2015**, *3*, 11660-11674.

(47) Kohn, W.; Sham, L. J. Self-Consistent Equations Including Exchange and Correlation Effects. *Phys. Rev.* **1965**, *140*, A1133–A1138.

(48) Lee, C.; Yang, W.; Parr, R. G. Development of the Colle-Salvetti Correlation-Energy Formula into a Functional of the Electron Density. *Phys. Rev. B* **1988**, *37*, 785–789.

(49) Becke, A. D. Density-Functional Thermochemistry. III. The Role of Exact Exchange *J. Chem. Phys.* **1993**, *98*, 5648–5652.

(50) Gross, E. K. U.; Kohn, W. Local Density-Functional Theory of Frequency-Dependent Linear Response *Phys. Rev. Lett.* **1985**, *55*, 2850–2852.

(51) Gross, E. K. U.; Kohn, W. Time-Dependent Density-Functional Theory. *Adv. Quantum Chem.* **1990**, *21*, 255–291.

(52) Bauernschmitt, R.; Ahlrichs, R. Treatment of Electronic Excitations within the Adiabatic Approximation of Time Dependent Density Functional Theory. *Chem. Phys. Lett.* **1996**, *256*, 454–464.

(53) Casida, M. E.; Jamorski, C.; Casida K. C.; Salahub, D. R. Molecular Excitation Energies to High-Lying Bound States from Time-Dependent Density-Functional Response Theory: Characterization and Correction of the Time-Dependent Local Density Approximation Ionization Threshold. *J. Chem. Phys.* **1998**, *108*, 4439–4449.

(54) Dennington, R.; Keith, T.; Millam, J. GaussView, Version, 5, Semichem Inc., Shawnee Mission KS, 2009.

(55) Bredas, J. L.; Beljonne, D.; Coropceanu, V.; Cornil, J. Charge-Transfer and Energy-Transfer Processes in pi-Conjugated Oligomers and Polymers: a Molecular Picture. *Chem. Rev.* **2004**, *104*, 4971–5003.

(56) Frisch, M. J.; Trucks, G. W.; Schlegel, H. B.; Scuseria, G. E.; Robb, M. A.; Cheeseman, J. R.; Scalmani, G.; Barone, V.; Mennucci, B.; Petersson, G. A.; Nakatsuji, H.; Caricato, M.; Li, X.; Hratchian, H. P.; Izmaylov, A. F.; Bloino, J.; Zheng, G.; Sonnenberg, J. L.; Hada, M.; Ehara, M.; Toyota, K.; Fukuda, R.; Hasegawa, J.; Ishida, M.; Nakajima, T.; Honda, Y.; Kitao, O.; Nakai, H.; Vreven, T.; Montgomery, J. A., Jr.; Peralta, J. E.; Ogliaro, F.; Bearpark, M.; Heyd, J. J.; Brothers, E.; Kudin, K. N.; Staroverov, V. N.; Kobayashi, R.; Normand, J.; Raghavachari, K.; Rendell, A.; Burant, J. C.; Iyengar, S. S.; Tomasi, J.; Cossi, M.; Rega, N.; Millam, J. M.; Klene, M.; Knox, J. E.; Cross, J. B.; Bakken, V.; Adamo, C.; Jaramillo, J.; Gomperts, R.; Stratmann, R. E.; Yazyev, O.; Austin, A. J.; Cammi, R.; Pomelli, C.; Ochterski, J. W.; Martin, R. L.; Morokuma, K.; Zakrzewski, V. G.; Voth, G. A.; Salvador, P.; Dannenberg, J. J.; Dapprich, S.; Daniels, A. D.; Farkas, Ö.; Foresman, J. B.; Ortiz, J. V.; Cioslowski, J.; Fox, D. J. Gaussian, Inc., Wallingford CT, 2009.

(57) Honmou, Y.; Hirata, S.; Komiyama, H.; Hiyoshi, J.; Kawauchi, S.; Iyoda, T.; Vacha, M. Single Molecule Electroluminescence and Photoluminescence of Polyfluorene Unveils the Photophysics Behind the Green Emission Band. *Nat. Commun.* **2014**, *5*, 4666.

(58) Inoue, H.; Hida, M.; Nakashima, N.; Yoshihara, K.; Picosecond Fluorescence Lifetimes of Anthraquinone Derivatives. Radiationless Deactivation via Intra- and Intermolecular Hydrogen Bonds. *J. Phys. Chem.* **1982**, *86* (16), 3184–3188.

(59) Ng, T.W.; Lo, M.F.; Fung, M.K.; Zhang, W.J.; Lee, C.S. Charge-Transfer Complexes and Their Role in Exciplex Emission and Near-Infrared Photovoltaics. *Adv. Mater.* **2014**, *26*, 5569–5574.

(60) Naka, S.; Okada, H.; Onnagawa, H.; Tsutsui, T. High Electron Mobility in Bathophenanthroline. *Appl. Phys. Lett.* **2000**, *76* (2), 197–199.

(61) Lee, J.; Chen, H.F.; Batagoda, T.; Coburn, C.; Djurovich, P.I.; Thompson, M.E.; Forrest, S.R. Deep Blue Phosphorescent Organic Light-Emitting Diodes with Very High Brightness and Effciency. *Nat. Mater.* **2015**, DOI: 10.1038/NMAT4446.

(62) Tsai, T.C.; Hung, W.Y.; Chi, L.C.; Wong, K.T.; Hsieh, C.C.; Chou, P.T. A New Ambipolar Blue Emitter for NTSC Standard Blue Organic Light-Emitting Device. *Org. Electron.* **2009**, *10*, 158−162.

(63) Cook, J.H.; Santos, J.; Li, H.; Al-Attar, H.A.; Bryce, M.R.; Monkman, A.P. Efficient Deep Blue Fluorescent Polymer Lightemitting Diodes (PLEDs). *J. Mater. Chem. C*, **2014**, *2*, 5587-5592.